

## **Abstract**

A three-dimensional microwave tomography (3-D imaging) system prototype, using continuous wave near field techniques, operation at 5.8 GHz, has been designed and built. The system is mainly intended to be used in food industry for measuring temperature (of chicken breast, hamburger... etc.) and detecting foreign bodies in food products (baby food, bread loaf...etc.), but it can be used for medical examination purposes or for various industrial applications as well. Almost 2000 measurements had been conducted. An accuracy of  $\pm 5$  °C in temperature measurements and detecting a glass sphere of 2 mm in diameter in a bread loaf, were achieved.

# Contents

Abstract	1
1 Introduction	3
2 Theory of Microwave Tomography	4
2.1 Analysis	4
2.1.1 The Forward Problem	4
2.1.2 The Inverse Problem	6
3 System Description	8
4 Antenna Systems	9
4.1 Microstrip Patch Antennas	10
4.1.1 Method of Analysis	12
4.1.2 Design and Simulation	14
5 RF Amplifier	16
5.1 Analysis	16
5.1.1 Bias Circuit	16
5.2 Construction	17
6 Directional Coupler	18
6.1 Analysis	18
6.2 Simulation	19
6.3 Construction	20
7 Mixer	21
7.1 Analysis	21
7.1.1 Biasing	22
7.1.2 Impedance matching	24
7.1.3 Stepped impedance lowpass filter	25
7.2 Simulation	27
7.3 Construction	27
8 Active Bandpass Filter	29
8.1 Analysis	29
8.2 Simulation	30
8.3 Construction	30
9 Signal Processing	32
9.1 Analog to Digital Converter, AD6600	33
9.2 Digital Signal Processing, AD6620	34
9.2.1 Digital filter design	35
9.3 Software	36
9.3.1 Structure of the interface	36
10 Synchronisation	38
11 Power Supply	39
12 Results	40
13 Conclusions	42
14 References	43

# 1 Introduction

The tomography is generally perceived as an imaging tool either for medical examination purposes or for various industrial applications. Presently there are a number of tomographic techniques available, e.g., infrared, optical, X-ray tomographic systems and so on.

The objective of microwave tomography is to reconstruct the dielectric properties of an object illuminated with microwaves from a measurement of the scattered fields. The overall reconstruction process in general involves the measurement of scattering data such as the reflection coefficient of an illuminating wave with known characteristics. Information about the unknown permittivity profile of the illuminated object in terms of these measured values is obtained by using some inverse techniques.

The objectives of this master thesis work were to construct and validate a 3-dimensional microwave tomography (sensor) prototype, to be used in food industry for temperature measurements and/or detection of foreign bodies in food material. Foreign body contamination is of great concern to food companies. A foreign body incident can jeopardise consumer health, result in prosecution and significantly undermine a company's reputation. However, such a sensor is desired to increasing quality control and reducing customer complaints.

The sensor uses low power microwaves in the lower milliwatt range. The emitted microwave is collected by an antenna array. There is electronics to determine the power level and the delay between the emitted microwave and the collected signal. The measurement data is processed and filtered.

The antennas are mounted close to a conveyor belt where e.g. chicken breasts are transported. Using the translational motion of the belt and the time information given by the sensors, a matrix of microwave information is generated on-line.

Presently X-ray tomography is used in food industry for detection of foreign bodies in food material, but it is regarded as a considerable investment for small companies, besides it is not particularly reliable.

## 2 Theory of Microwave Tomography

The aim of microwave tomography is to obtain information regarding the inside of an object using microwave technology. In this project both the forward method and the inverse scattering method were considered.

### 2.1 Analysis

Before going into more detail of the forward and the inverse problem the following definitions of the field in the object and in the sensor have to be defined.

Assume that  $M$  antennas are placed out at given locations  $\mathbf{r}_i$  forming the sensor domain  $\Omega$  with known dielectric contrasts collected in a vector  $C_\Omega = \mathbf{e}_{r,\Omega} - 1$  and a medium described by a contrast function  $c(\mathbf{r}) = \mathbf{e}_r - 1$ . The medium is discretized by  $N = n \times n$  dielectric contrast sources summarized as  $C_0 = \mathbf{e}_{r,0} - 1$  assuming a vacuum background. Then the fields in the medium and in the sensors are obtained using a Green's function approach:

$$E_0(\mathbf{r}) = E_0^i(\mathbf{r}) + \int_{0,\Omega} G(\mathbf{r}, \mathbf{r}') c(\mathbf{r}') E(\mathbf{r}') dO + \sum_{\Omega} \int_j G(\mathbf{r}, \mathbf{r}_j) c_{\Omega}(j) E(\mathbf{r}_j) d\Omega \quad (1)$$

$$E_\Omega(\mathbf{r}_i) = E_\Omega^i(\mathbf{r}_i) + \int_{0,\Omega} G(\mathbf{r}_i, \mathbf{r}') c(\mathbf{r}') E(\mathbf{r}') dO + \sum_{\Omega} \int_j G(\mathbf{r}_i, \mathbf{r}_j) c_{\Omega}(j) E(\mathbf{r}_j) d\Omega \quad (2)$$

Equation 1 shows the total field in the object at an arbitrary point. The first term is the incident field at the point. The second term is the scattered field in the point which is caused by the adjacent points. The third term is the total field from the mutual current of the receiver antennas on the observation point.

Equation 2 describes the total field at a certain point in the receiver antenna region. The first term is the incident field at the sensor at the point and the second term is the field at the point which is the scattered field of the object. The third term is the total field at the point, caused by the mutual current of the receiver antennas.

#### 2.1.1 The Forward Problem

The forward problem gives information about the field in the object,  $E_0$ . This method is appropriate for the *foreign body in food* sensor application.

To compare the approach with standard techniques described in literature the sensor contrasts are set identical to zero.

$$E_0 = E_0^i + \overline{K_{00}} \cdot \overline{C_0} \cdot E_0 \quad (3)$$

$$E_\Omega = E_\Omega^i + \overline{K_{\Omega 0}} \cdot \overline{C_0} \cdot E_0 \quad (4)$$

The field at the sensors without any medium in the measurement gap becomes:

$$E_\Omega^\# = E_\Omega^i \quad (5)$$

The scattered field at the sensors is determined by the difference of the fields with and without the medium present

$$E_\Omega^s = E_\Omega - E_\Omega^\# \quad (6)$$

Since the basis relations are usually given in terms of the complete field at the medium and the scattered field at the sensors the basic relations become therefore:

$$E_0 = E_0^i + \overline{K_{00}} \cdot \overline{C_0} \cdot E_0 \quad (7)$$

$$E_\Omega^s = \overline{K_{\Omega 0}} \cdot \overline{C_0} \cdot E_0 \quad (8)$$

Medium equation 7 is used to solve the forward problem:

$$E_0^i = \left( \overline{1} - \overline{K_{00}} \cdot \overline{C_0} \right) \cdot E_0 \quad (9)$$

Solving equation 9 results in an expression for the field in the medium (index O) as a function of the incident field when the contrast is known.

$$E_0 = \left( \overline{1} - \overline{K_{00}} \cdot \overline{C_0} \right)^{-1} \cdot E_0^i = \overline{H} \cdot E_0^i \quad (10)$$

Formally an inverse forward matrix is defined as follows:

$$\overline{H} = \left( \overline{1} - \overline{K_{00}} \cdot \overline{C_0} \right)^{-1} \quad (11)$$

In the foreign body detection application when  $E_\Omega^s$  is not equal to 0 the object is contaminated. To be able to identify the foreign body, the first step is to assume that the material is known, which means that  $\overline{K_{00}}$  and  $\overline{C_0}$  are known. Then  $\overline{H}$  can be calculated from equation 11. If that  $\overline{H}$  makes  $E_\Omega^s$  in equation 6 zero, the predicted material is the desired material. If not, the procedure has to be repeated.

## 2.1.2 The Inverse Problem

The inverse problem is that by knowing the changes in the scattered field  $dE_{\Omega}^s$  at the receiver antenna region, information of the material in the object can be obtained. The temperature sensor is an example of a sensor that uses this technique.

Here the source-medium interactions are not included. The basis relations are a medium equation and an antenna or source equation. The medium equation 7 and the sensor equation 8 are now solved for differential changes in the contrast resulting in differential changes of the scattered field at the sensors.

$$E_0^i = E_0 + \overline{K_{00}} \cdot \overline{C_0} \cdot E_0 \quad (12)$$

$$dE_{\Omega}^i = 0 \quad (13)$$

$$0 = dE_0 - \overline{K_{00}} \cdot d(\overline{C_0} \cdot E_0) \quad (14)$$

$$dE_0 = \overline{K_{00}} \cdot d(\overline{C_0} \cdot E_0) \quad (15)$$

According to the rules of derivation  $d(\overline{C_0} \cdot E_0)$  becomes:

$$d(\overline{C_0} \cdot E_0) = d\overline{C_0} \cdot E_0 + \overline{C_0} \cdot d(E_0) \quad (16)$$

Inserting equation 15 in equation 16 gives:

$$d(\overline{C_0} \cdot E_0) = d\overline{C_0} \cdot E_0 + \overline{C_0} \cdot \overline{K_{00}} \cdot d(\overline{C_0} \cdot E_0) \quad (17)$$

$$d(\overline{C_0} \cdot E_0) \cdot (1 - \overline{C_0} \cdot \overline{K_{00}}) = d\overline{C_0} \cdot E_0 \quad (18)$$

Solving this equation for  $d(\overline{C_0} \cdot E_0)$  results in:

$$d(\overline{C_0} \cdot E_0) = d\overline{C_0} \cdot E_0 \cdot (1 - \overline{C_0} \cdot \overline{K_{00}})^{-1} \quad (19)$$

Starting with sensor equation 8, one obtains for small changes in the contrast:

$$E_{\Omega}^s = \overline{K_{\Omega 0}} \cdot \overline{C_0} \cdot E_0 \quad (8)$$

$$dE_{\Omega}^s = \overline{K_{\Omega 0}} \cdot d(\overline{C_0} \cdot E_0) \quad (20)$$

Inserting the expression for  $\mathbf{d}(\overline{C_0} \cdot E_0)$  in 20 results:

$$\mathbf{d}E_{\Omega}^s = \overline{K_{\Omega 0}} \cdot \mathbf{d}\overline{C_0} \cdot E_0 \cdot \left(1 - \overline{C_0} \cdot \overline{K_{00}}\right)^{-1} \quad (21)$$

$$\mathbf{d}E_{\Omega}^s = \overline{K_{\Omega 0}} \cdot \mathbf{d}\overline{C_0} \cdot E_0 \cdot \overline{H} \quad (22)$$

$$\mathbf{d}E_{\Omega}^s = \overline{K_{\Omega 0}} \cdot \overline{H} \cdot \overline{1} \cdot \mathbf{d}\overline{C_0} \cdot E_0 \quad (23)$$

$$\mathbf{d}E_{\Omega}^s = \overline{K_{\Omega 0}} \cdot \overline{E_0} \cdot \overline{H} \cdot \mathbf{d}\overline{C_0} \quad (24)$$

The definition of the sensitivity matrix  $\overline{D}$  becomes:

$$\overline{D} = \overline{K_{\Omega 0}} \cdot \overline{H} \cdot \overline{E_0} = \overline{K_{\Omega 0}} \cdot \left(1 - \overline{C_0} \cdot \overline{K_{00}}\right) \cdot \overline{E_0} \quad (25)$$

Then the matrix equivalent of the differential inverse problem which must be solved for an inverse scattering solution is the following:

$$\mathbf{d}E_{\Omega}^s = \overline{D} \cdot \mathbf{d}\overline{C_0} \quad (26)$$

In conclusion, to solve the inverse problem is to iteratively go through the forward problem while changed  $e$ , which means  $C_0$ , in order to minimize the error between the measured scattered field  $E_{\Omega}^s$  and the scattered field  $E_{\Omega}^s$  estimated from a numerical model. The step will repeat until the error becomes zero, and then right  $e$  has been found. In the temperature sensor the  $e$  of water in an object will yield information about the temperature of the object.

Studying the interaction of microwaves and material, one finds that the only relevant microwave loss mechanism in organic materials is found in the contribution of free liquid water. The microwave properties (e.g. index of refraction and attenuation) of water are strongly temperature dependent. For any food material, the relative contents of water and the temperature of the water are the dominating parameters determining its microwave properties.

The microwave contrast data generated by the sensor contains all relevant data to localize the different constituents and in to assign a temperature to these constituents. The better the water and salt contents of the constituents is known the more accurate the temperature measurement becomes.

The temperature can be obtained in all products that containing liquid, free water. This is the case for all food material consisting of cellular material as long as the product is not deep frozen or completely dried.

### 3 System Description

The system is consisting of three major units, transmitter unit, receiver unit and the signal processing unit. Figure 1 is a graphical depiction of the system schematic.

The transmitter unit consists of a microwave generator that generates a signal with 12 dBm as a maximum, this signal will be amplified by the RF amplifier. The directional coupler will pass the major part of the effect to the transmitter antenna and the rest will be used as reference signal to conduct system calibration.

The receiver unit consists of a receiver antenna, a microwave generator acts as a local oscillator for the active mixer, which mixes down the RF signal coming from the antenna, the resulting IF signal will be filtered by the mean of an active filter to compensate for the attenuation.

The filtered signal will be fed to the signal processing's unit via a dual-channel IF sampling analogue-to-digital converter. The digitized signal will go through a digital signal-processing unit (DSP), then the data will be transmitted to a computer via a parallel port to make the final processing by running some sort of inverse scattering scheme.

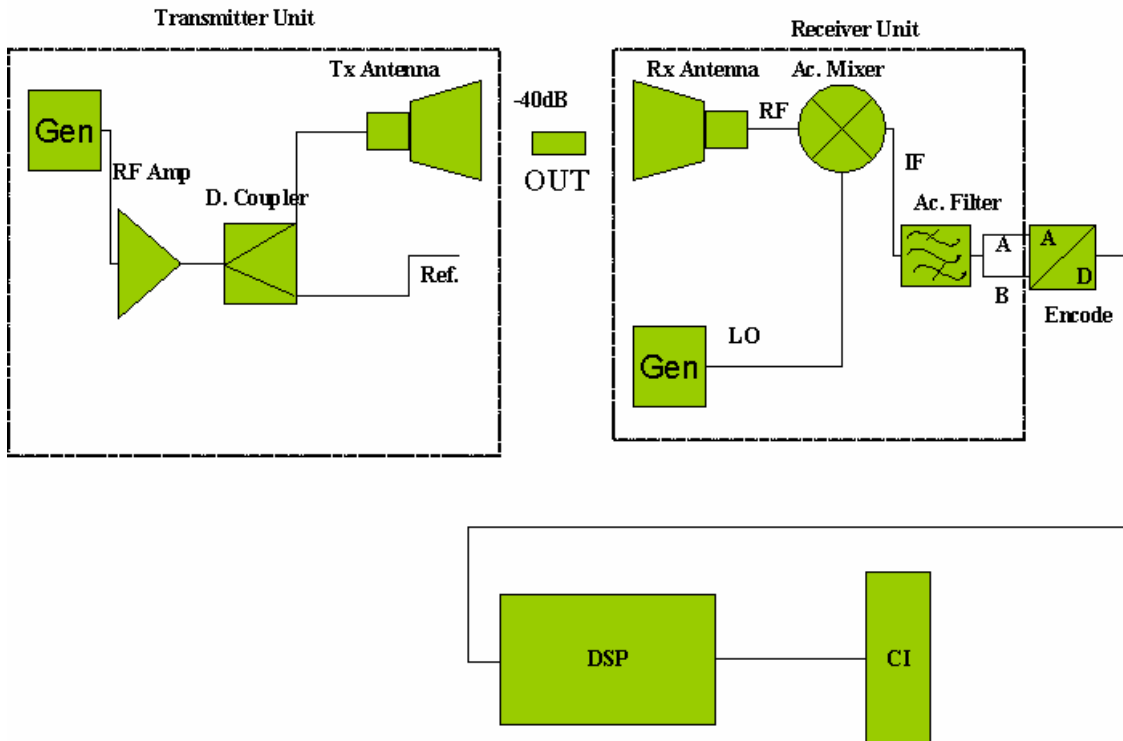


Figure 1 System schematic

## 4 Antenna Systems

An antenna is a structure for radiating or receiving electromagnetic (EM) waves that carry information. For wireless applications, EM signals are not sent through a transmission line, and, therefore, antennas are required for the transmission and reception of the signals.

The design of the antenna system is very important in a transmitting unit. The antenna must be able to radiate efficiently so the power supplied by the transmitter is not wasted. An efficient transmitting antenna must have exact dimensions. The dimensions are determined by the transmitting frequencies. The dimensions of the receiving antenna are not critical for relatively low radio frequencies. However, as the frequency of the signal being received increases, the design and installation of the receiving antenna become more critical.

There are various types of antennas. However, to decide whether a certain antenna is suitable for a wireless application, many aspects should be taken into account, among others, cost, surface, polarization, radiation pattern and so on.

The radiation pattern of an antenna has a near field and a far field se Figure 2. The near field is composed of electric and magnetic force fields. This holds true to about 4 wavelengths from the radiator, and then the predominate radiation is the electromagnetic field. The boundary between the near and far fields is an arbitrary sphere surrounding the antenna whose radius  $R_{ff}$  is

$$R_{ff} = \frac{2 D^2}{\lambda}$$

Where  $\lambda$  is the wavelength of the radiation and  $D$  is the physical linear dimension of the antenna. The radiation patterns that describe the radiation intensity of the antenna as a function of angle are usually patterns for the far field.

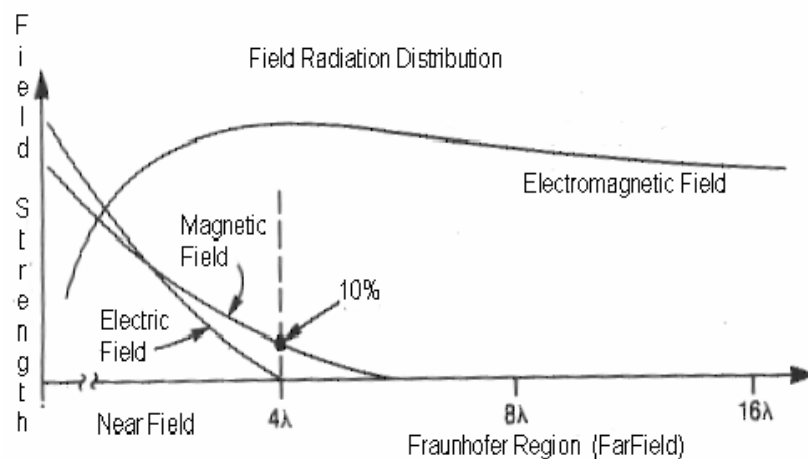


**Figure 2 Near field and far field for antenna**

For the purpose of microwave tomography, the near field of the antenna is used. This will guarantee that the object under test will be scanned with out any blind spots, and make it possible to detect foreign bodies with very small dimensions down to 2 mm.

#### **4.1 Microstrip Patch Antennas**

For this system, the decision had been made to make use of microstrip antennas, because, these antennas are low profile, low-cost and support the operation of many modern microwave systems. Versatile in terms of resonant frequency, polarization, pattern, and impedance. Microstrip patch antennas represent one family of compact antennas that offers the benefits of a conformal nature and the capability of ready integration with a microwave system's printed circuitry, mechanically robust when mounted on rigid surface.

The patch antennas consist of a metallic patch etched on a dielectric substrate se Figure 3, which has a grounded metallic plane at the opposite side. They are developed in the beginning of 1970s. There is great variety of geometries and ways of excitation.

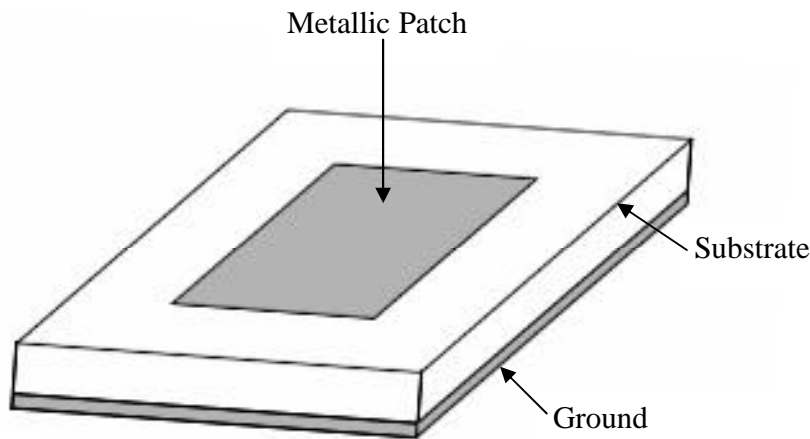


**Figure 3 Microstrip patch antenna**

The patch antenna is essentially a rectangular dipole. The patch antenna is a relatively narrowband antenna. In the square configuration it radiates a linearly polarized wave. Feeding and impedance matching is accomplished in a number of ways. The patch can be matched with a quarter wave high impedance line, or a  $50\ \Omega$  line can be extended into the interior of the patch, as shown below in Figure 4. The impedance is minimum at the centre and increases along the axis, so the choice of dimension is made to attach to the  $50\ \Omega$  point. This method is used in our design and will be explained later on.

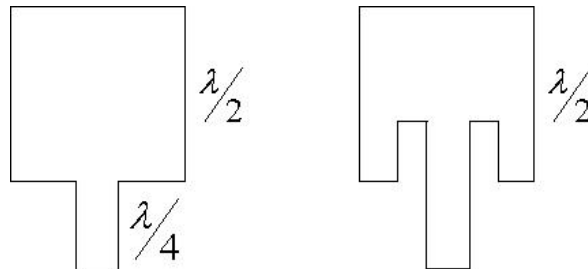


**Figure 4 Microstrip line feed**

An alternate feed method is to bring the centre conductor of a coaxial line through the dielectric to contact the underside of the patch at the appropriate impedance point. The centre of the patch is grounded with a via in this configuration, as shown in Figure 5 as left and centre. The patch can also be used to generate a circularly polarized wave by making the two side dimensions unequal to form a rectangle as shown below right. The feed is connected along a diagonal from the centre to the corner, with the dimension chosen for an impedance match.

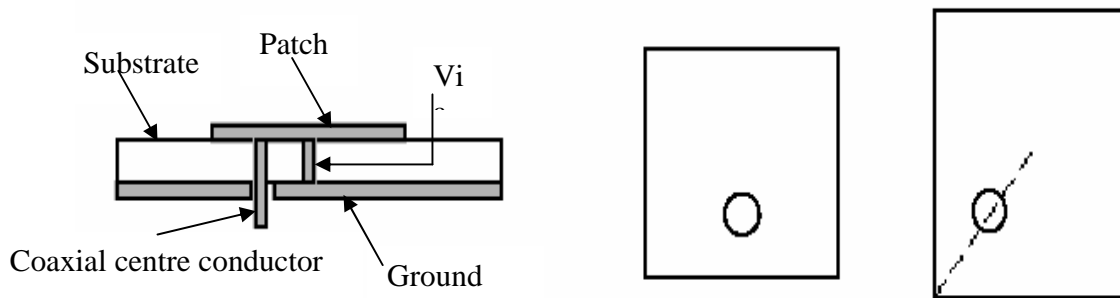


Figure 5: Coaxial feed

#### 4.1.1 Method of Analysis

The transmission-line model is regarded as one of the most popular methods of analysis for microstrip antennas. However, there are some more methods used for the same purpose, among others, the cavity and the full-wave. Each of the above mentioned methods has its own advantages and disadvantages. The transmission-line method is the easiest of all, it gives good physical insight, but is less accurate and is more difficult to model coupling. The cavity model is more accurate but at the same time more complex. However it also gives good physical insight and is rather difficult to model coupling.

In this thesis work, the transmission-line model had been used to analyze the rectangular patch antenna which is the most widely used configuration.

#### Transmission-Line Model

Basically the transmission-line model represents the microstrip antenna by two slots, separated by a low-impedance  $Z_c$  transmission line of length  $L$ . Because the dimensions of the patch are finite along the length and the width, the fields at the edges of the patch undergo fringing. The amount of fringing is a function of the dimensions of the patch and the height of the substrate  $h$ . For the principal  $E$ -plane fringing is a function of the ratio of the length of the patch  $L$  to the height  $h$  of the substrate ( $L/h$ ) and the dielectric constant  $\epsilon_r$  of the substrate. Fringing must be taken into account because it influences the resonant frequency of the antenna.

For a microstrip line shown in Figure 6(a), typical electric field lines are shown in Figure 6(b). This is a nonhomogeneous line of two dielectrics, the substrate and the air. Most of the electric field lines reside in the substrate and parts of some lines exit in air. Fringing in this case makes the microstrip line look wider electrically compared to its physical dimensions. Since some of the waves travel in the substrate and some in the air, an effective dielectric constant  $e_{\text{reff}}$  is introduced to account for fringing and the wave propagation in the line.

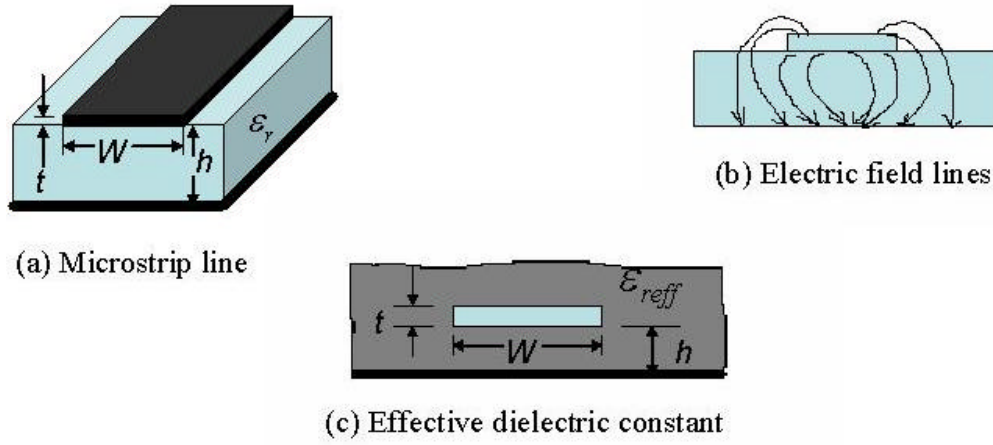


**Figure 6: Microstrip line and its electric field lines, and effective dielectric constant geometry**

$$\epsilon_{eff} = \frac{\epsilon_r + 1}{2} + \frac{\epsilon_r - 1}{2} \left[ 1 + 12 \frac{h}{W} \right]^{-1/2}$$

Where  $\epsilon_r$  is the dielectric constant of the substrate,  $h$  is the thickness of the substrate, and  $W$  is the width of the patch.

The effective length of the patch antenna  $L_{eff}$  is greater than its physical, because of the fringing effect.

$$L_{eff} = L + 2\Delta L$$

$$\frac{\Delta L}{h} = 0.412 \frac{(\epsilon_{eff} + 0.3) \left( \frac{W}{h} + 0.264 \right)}{(\epsilon_{eff} - 0.258) \left( \frac{W}{h} + 0.8 \right)}$$

The width of the patch  $W$  could be calculated as below:

$$W = \frac{1}{2f_r \sqrt{\mu \epsilon_0}} \sqrt{\frac{2}{\epsilon_r + 1}} = \frac{c_0}{2f_r} \sqrt{\frac{2}{\epsilon_r + 1}}$$

Where  $c_0$  is the free space velocity of light, and  $f_r$  is the resonant frequency.

The feed mechanism plays an important role in the design of microstrip patch antennas. As it's mentioned earlier, the microstrip line feed is used in the design. The inset length  $y_0$  determines the input impedance. It has been found experimentally that on low-dielectric-constant materials, the input impedance of an inset-fed probe antenna exhibits fourth-order behavior following the function:  $\cos^4 [\mathbf{p}(y_0 / L)]$ .

Fortunately, a simple analytical approach has been developed using the transmission-line model to find the input impedance of an inset-fed microstrip patch antenna. Using this approach, a curve-fit formula can be derived

to find the inset length to achieve  $50 \Omega$  input impedance when using modern thin dielectric circuit-board materials.

The input impedance of an inset-fed microstrip patch antenna depends mainly on the inset distance,  $y_0$ , and to some extent on the inset width,  $w_f$  (the spacing between the feed line and the patch conductor). Variations in the inset length do not produce any change in resonant frequency, but a variation in the inset width will result in a change in resonant frequency.

The curve-fit formula to find the exact inset length to achieve  $50 \Omega$  input impedance for commonly used thin dielectric substrates ( $2 \leq \epsilon_r \leq 10$ ) is described below:

$$y_0 = 10^{-4} \{0.001699\epsilon_r^7 + 0.13761\epsilon_r^6 - 6.1783\epsilon_r^5 + 93.187\epsilon_r^4 - 682.69\epsilon_r^3 + 2561.9\epsilon_r^2 - 4043\epsilon_r + 6697\}$$

#### 4.1.2 Design and Simulation

The above mentioned method has been used to design the antennas for our microwave tomography system. However, a 3D electromagnetic analysis and design software tool been utilised to conduct the simulation and enhance the design. The software called Micro-Stripes and it is based on the TLM (Transmission Line Matrix).

Microstrip patch antennas at different operation (5.8 GHz and 9.9 GHz) frequencies have been designed and simulated. A set antennas, both receiver and transmitter antennas at 9.9 GHz have been built and mounted with the rest of the system se Figure 8 and 9. The performance was good and it has a relatively broadband. SMA connectors were used to connect the antenna to the system.

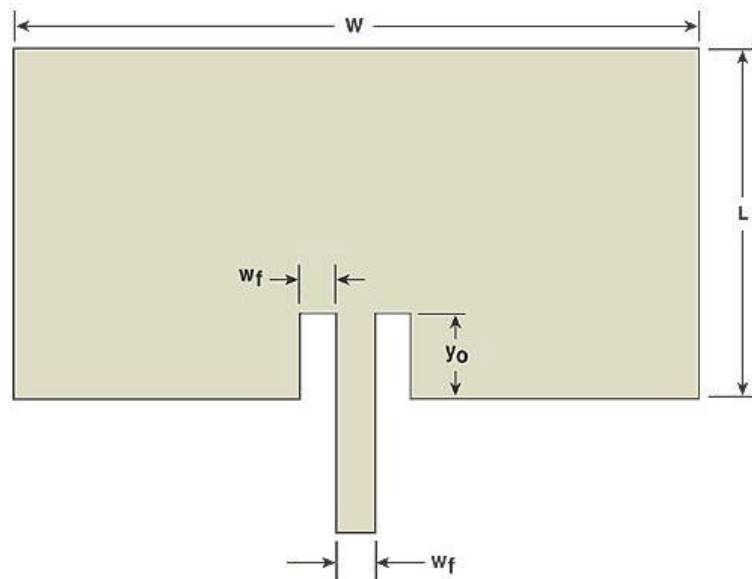
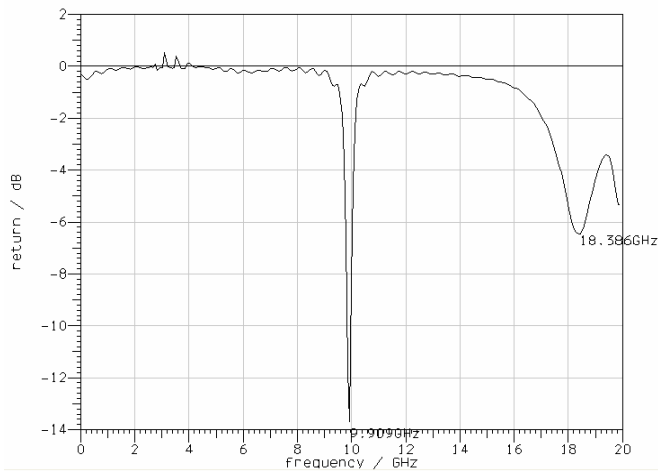
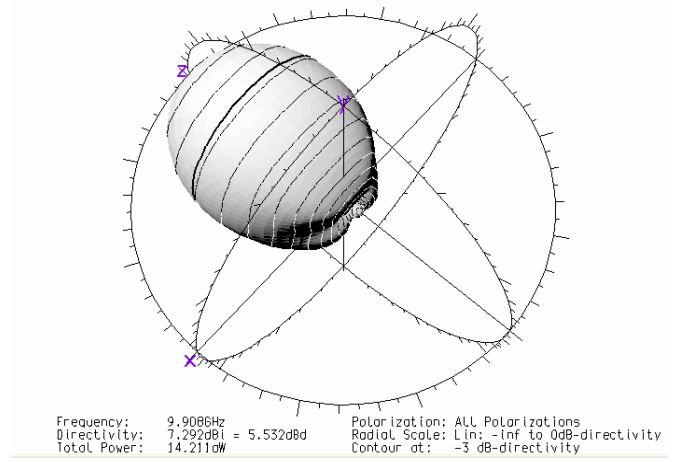


Figure 7 Patch parameters



(a) Return loss



(b) Radiation pattern

Figure 8: Return loss and radiation patter for the 9.9 GHz patch antenna

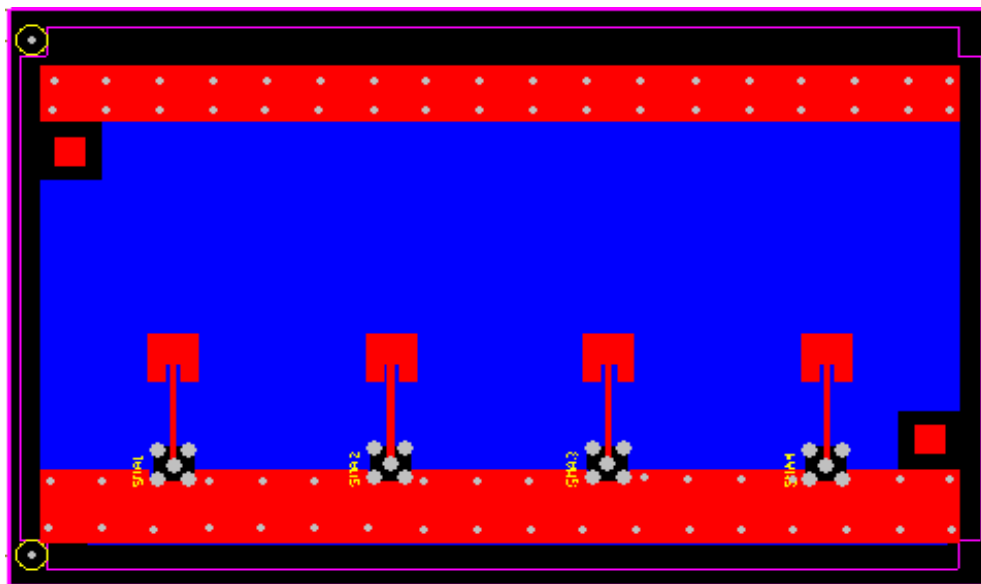


Figure 9 The layout for the 9.9 GHz patch antenna

## 5 RF Amplifier

Because of the attenuation of the system a RF amplifier is needed to provide a larger output power. To obtain the amplification an ERA-1 has been used.

### 5.1 Analysis

#### 5.1.1 Bias Circuit

The biasing configuration is shown in Figure 1. Bias current is delivered from a voltage supply  $V_{cc}$  through the resistor  $R_{bias}$  and the RF choke (inductor), shown as RFC in the Figure 10. The RF choke has been chosen such that its reactance is about  $500\ \Omega$  (10 times the load impedance) at the lowest operating frequency. In addition for better performance at high frequencies a quarter wave stripline has been used. The resistor reduces the effect of device voltage ( $V_{cc}$ ) variations on the bias current by approximating a current source.

Blocking capacitors are needed at the input and output ports. They are chosen as a type having a low ESR (effective series resistance), and have a reactance low enough not to affect insertion loss or VSWR (voltage standing wave ratio), adversely at low frequencies. The use of a bypass capacitor at the connection to the DC power supply prevents stray coupling to other signal processing components.

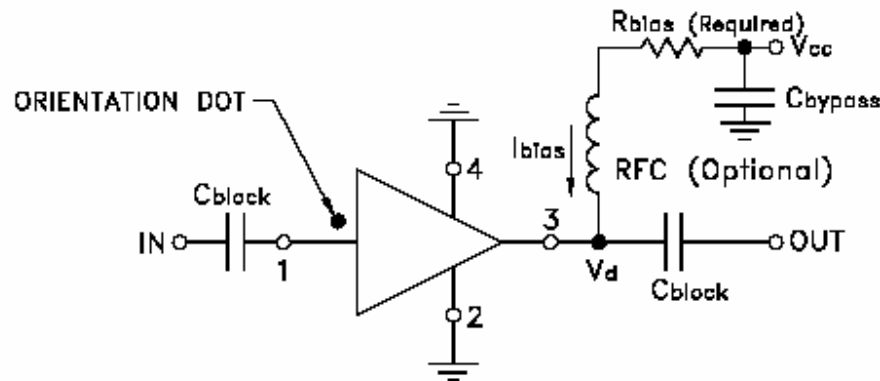


Figure 10: Typical biasing Configuration for ERA Amplifier

The bias current is given by the equation:

$$I_{bias} = \frac{V_{cc} - V_d}{R_{bias}}$$

The bias current values in Table 1 are the recommended values.

Improved ERA Model	ERA-1	ERA-2	ERA-21	ERA-3	ERA-33	ERA-4	ERA-50	ERA-51	ERA-6
Bias Current	40 mA	40 mA	40 mA	35 mA	40 mA	65 mA	60 mA	65 mA	70 mA
Device Voltage (nom.)	3.4V	3.5V	3.5V	3.2V	4.3V	4.5V	4.4V	4.5V	4.9V
Supply Voltage	Bias Resistor (ohms) at Supply Voltage								
7	90.9	88.7	88.7	107	69.8	38.3	47.5	40.2	30.1
8	113	113	113	133	93.1	52.3	63.4	53.6	43.2
9	137	137	137	162	115	66.5	78.7	68.1	56.2
10	162	162	162	191	140	80.6	95.3	82.5	69.8
11	187	187	187	221	165	95.3	113	97.6	84.5
12	215	215	210	249	191	110	127	113	97.6
13	237	237	237	280	215	127	143	127	113
14	261	261	261	309	243	143	162	143	127
15	287	287	287	340	267	158	178	158	140
16	309	316	316	365	287	174	196	174	154
17	332	340	340	392	316	187	210	191	169
18	357	365	365	422	340	205	226	205	182
19	383	392	392	453	365	221	243	221	196
20	412	412	412	475	392	237	261	237	210
Nominal dissip. in Resistor for 12V	0.34 W	0.34 W	0.34 W	0.31 W	0.31 W	0.51 W	0.45 W	0.50 W	0.52 W

Table 1: Bias resistor values for various supply voltages for the era amplifier series

## 5.2 Construction

The layout of the RF amplifier is made in Protel DXP as shown in Figure 11

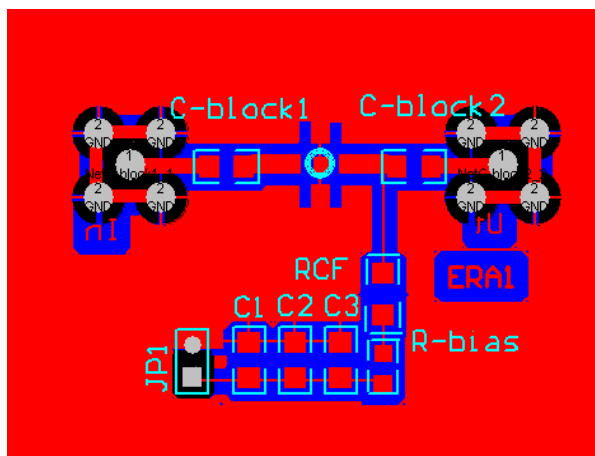


Figure 11: RF amplifier

## 6 Directional Coupler

Directional couplers physically consists of a pair parallel microstrip coupled transmission line, see Figure 12. Because of the interaction of the electromagnetic fields of each line, power can be coupled between the lines. The directional coupler are widely utilized for various RF and microwave applications because they can be easily be incorporated into and implemented with other circuits. However, the microstrip directional couplers suffer from poor directivity due to the characteristics of the inhomogeneous dielectric including both dielectric substrate and air in microstrip transmission lines. Thus, the phase velocity of even mode in microstrip is not equal to that of odd mode. The directivity performance of microstrip directional coupler becomes worse when the coupling is decreased or the dielectric permittivity is increased. In addition, it is difficult to achieve tight coupling owing to impractical spacing between the coupled lines in conventional edge coupled microstrip couplers.

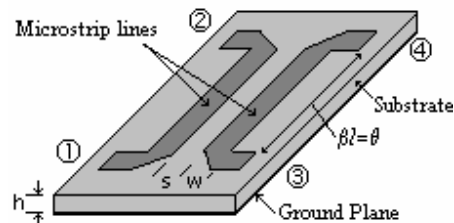


Figure 12: Microstrip Directional Coupler

### 6.1 Analysis

To obtain a reference signal as a part from the outgoing RF power a directional coupler is needed. The specification is:

Coupling:  $C = -20\text{dB}$

Power loss has to be very low

Characteristic impedance:  $Z_0 = 50\ \Omega$

PCB R3003:

Substrate thickness  $h = 1.55\ \text{mm}$

Metal thickness  $t = 35\ \mu\text{m}$

Relative substrate dielectric constant  $\epsilon_r = 4.7$

Because the parallel line couplers have different odd and even mode, and resulting different  $Z_{oe}$  and  $Z_{oo}$  (even and odd mode impedances respectively) so the first step in designing the coupler is to calculate these impedances. The equations that have been used are the following:

$$C = 10^{-C/20}$$

$$Z_{oe} = Z_o \sqrt{\frac{1+C}{1-C}} \quad \text{and} \quad Z_{oo} = Z_o \sqrt{\frac{1-C}{1+C}}$$

The parameters according to Figure 13 are then obtained by using the line calc subprogram in ADS.

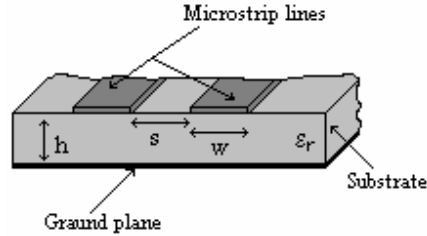


Figure 13: Coupled microstrip line

In order to provide maximum coupling the electrical length  $q$  of the microstrip line have to be  $l / 4$ .

## 6.2 Simulation

The simulation of the directional coupler has been done with the ADS program, as can be seen in Figure 15.

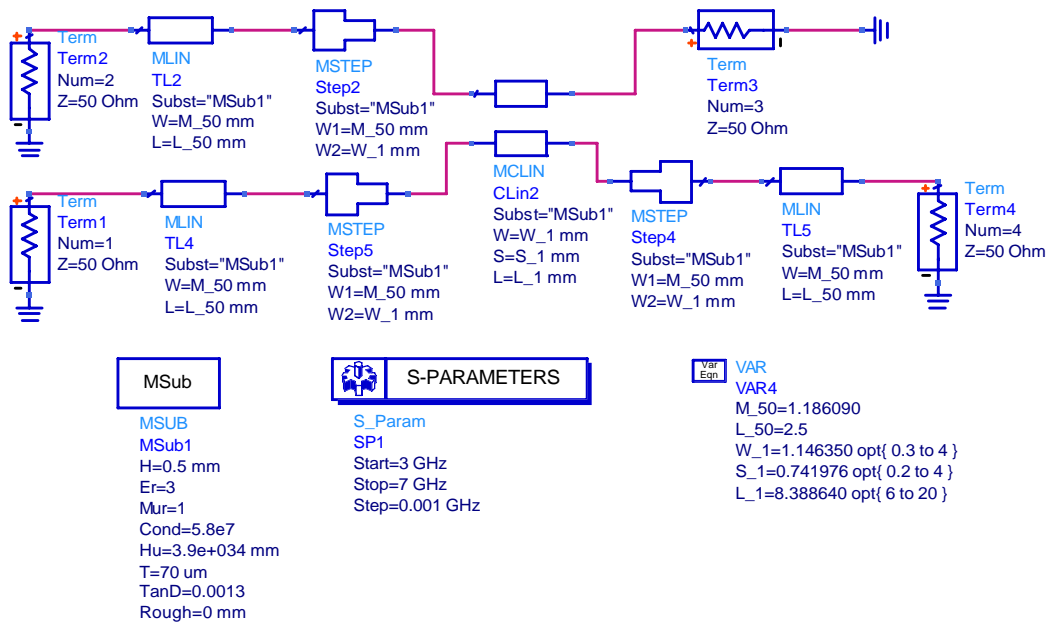


Figure 14: Simulation of the coupler

### Simulation of the directional coupler

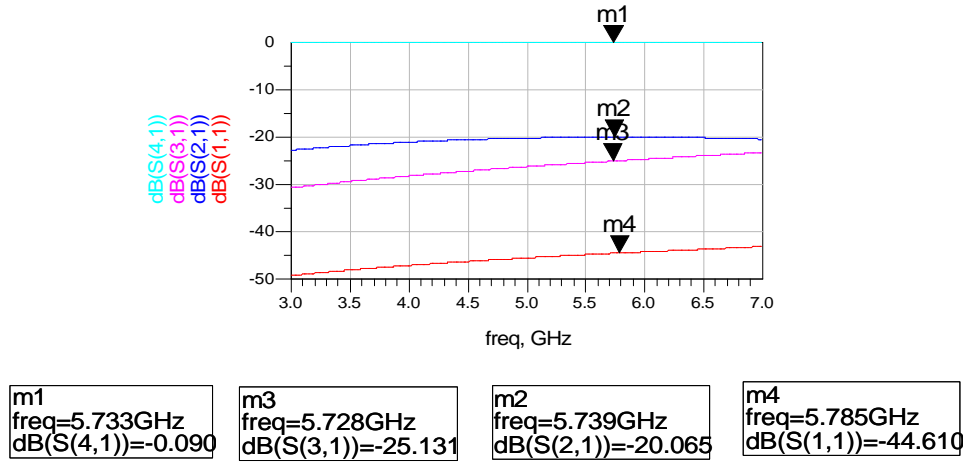


Figure 15: Simulation result of the directional coupler

### 6.3 Construction

According to the equation above the theoretical  $Z_{oe}$  and  $Z_{oo}$  are:

$$Z_{oe} = 55.2771 \Omega$$

$$Z_{oo} = 45.2267 \Omega$$

When the values of  $Z_{oe}$  and  $Z_{oo}$  are known the dimensions of the coupler can be calculated in ADS line calc, producing the following results:

$$L = 8.38864 \text{ mm}$$

$$W = 1.1464 \text{ mm}$$

$$S = 0.742 \text{ mm}$$

Then the layout of the directional coupler was designed in Protel DXP as shown in Figure 16

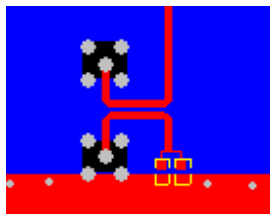


Figure 16: Layout of the D-Coupler

## 7 Mixer

The purpose of using a mixer in this system is to down-convert the RF signal to the IF signal on the receiver side. In order to balance the attenuation an active mixer is needed. The active mixer contains a transistor which is biased to obtain certain amplification.



Figure 17: Symbolic configuration of mixer

### 7.1 Analysis

Figure 17 shows a very simple symbol of a mixer. F1 is the RF frequency and F2 is the LO frequency. Because of the requirements on the down-converted signal like bandwidth, insertion loss and noise etc. even a lowpass filter has to be used at the output port.

The mixer contains a transistor of type BFR520 as seen in Figure 18.

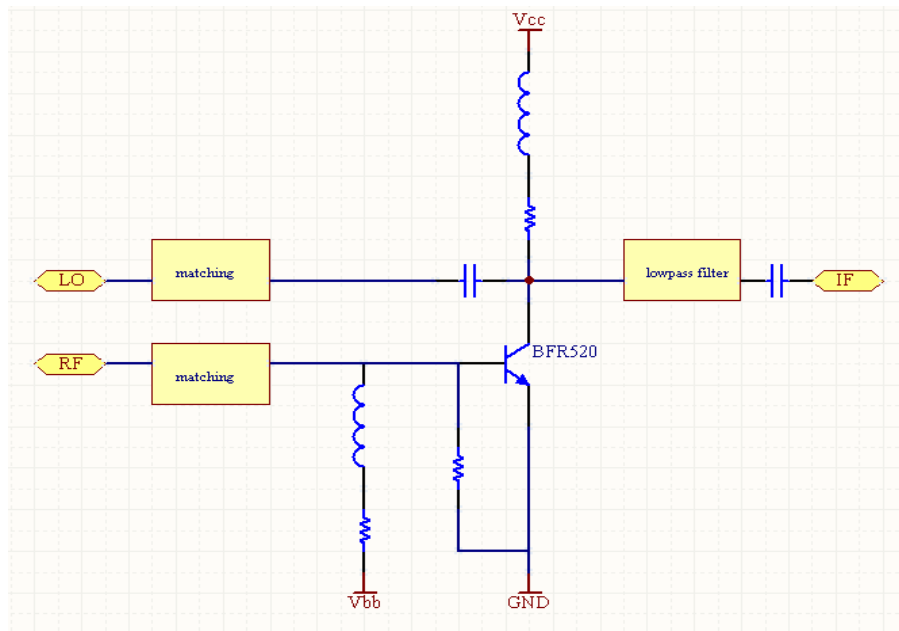
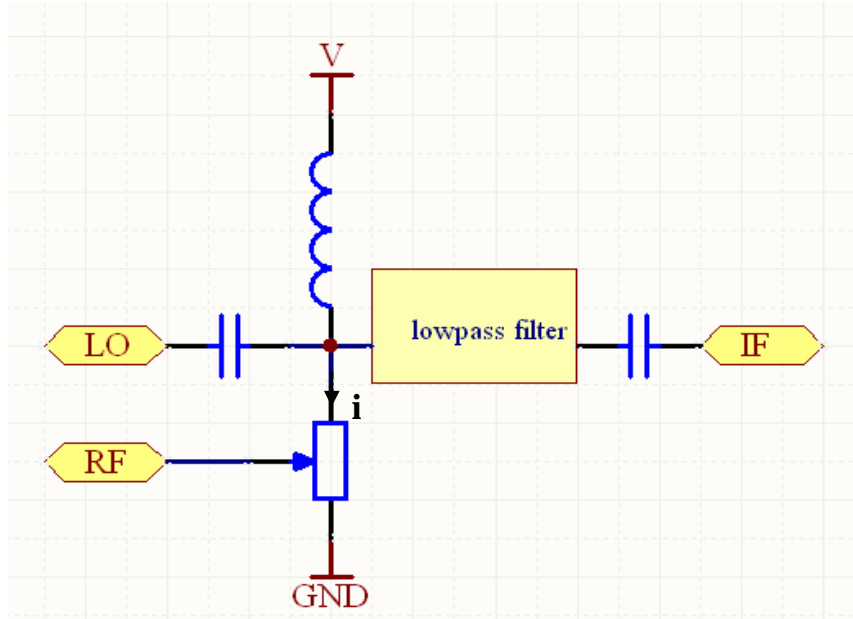


Figure 18: Mixer configuration



**Figure 19: Equivalent mixer**

Figure 19 shows the simplified model of the mixer configuration in Figure 18. This configuration is based on the following equation:

$$\begin{aligned}
 i &= \frac{V_0 \cos(\omega_2 t)}{R_0 + r \cos(\omega_1 t)} \\
 &= \frac{V_0 \cos(\omega_2 t)}{R_0} \\
 &= \frac{V_0}{R_0} \cos(\omega_2 t) \sum_{n=0}^{\infty} (-1)^n \frac{r}{R_0} \cos(\omega_1 t)
 \end{aligned}$$

Then the current,  $i$ , contains a product of  $\cos(\omega_2 t) \cos(\omega_1 t)$  which is characteristic for a mixer.

### 7.1.1 Biasing

The first step of the design is to make sure to know how the transistor behaves when the supply voltage varies. This was simulated in ADS using the model in Figure 20.

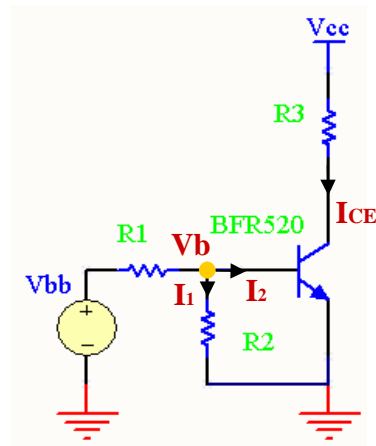


**Figure 20: Large signal analysis**

According to the stabilization of the transistor the followings can be assumed:

$$V_{bb} = 2V \quad V_b = 1V \quad V_{cc} = 10V \quad I_1 = 5mA \quad I_2 = 0.12mA \quad R_3 = 100\Omega$$

Then  $R_1$  and  $R_2$  become:

$$R_2 = \frac{V_b}{I_1} = 200\Omega$$

$$R_1 = \frac{V_{bb} - V_b}{I_1 + I_2} = 195\Omega$$

### **Simulation of the large signal analysis**

Figure 21 shows that to obtain  $I_{CE}$  equal to about 20mA, which is recommended in the datasheet for achieving the best performance of the transistor,  $R_2$  should be chosen to 135  $\Omega$ .

### Simulation of the biasing circuit

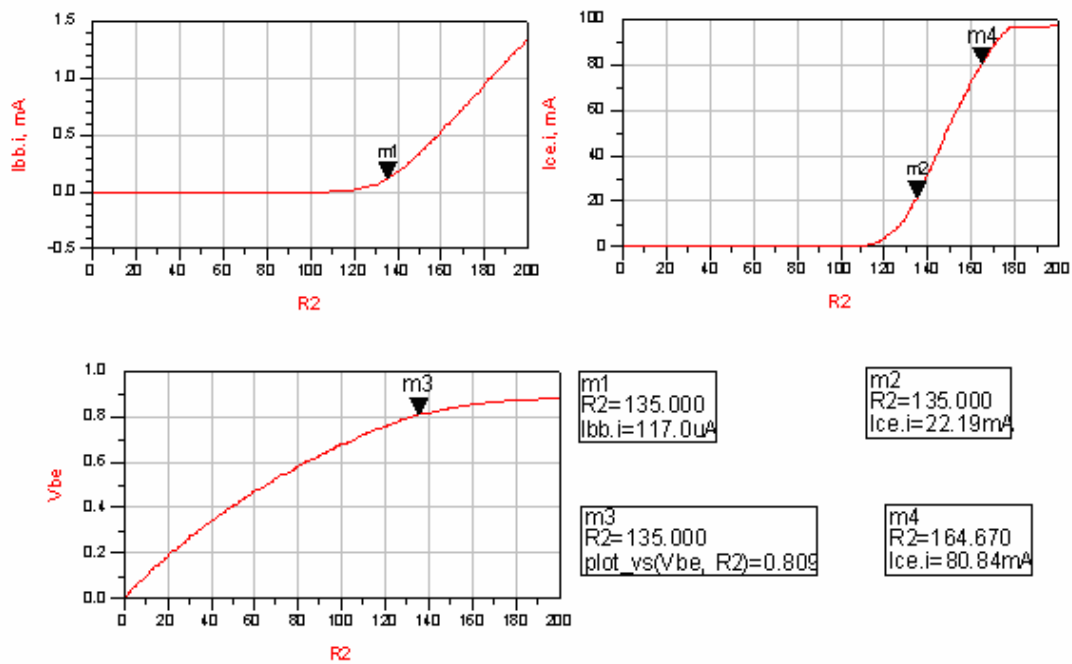


Figure 21: Simulation of biasing circuit

### 7.1.2 Impedance matching

RF and IF port mismatch is a major contributor to conversion loss, making impedance matching a very important step, especially when the level of the RF signal is very low.

To simplify the matching procedure an S-parameters simulation of the circuit can be made.  $S_{11}$ ,  $S_{22}$  and  $S_{33}$  can be obtained from the simulation graph. In order to provide a certain matching, the theoretical way by matching of using quarter wave stripline and conductors or inductors has been used. Figure 22 shows the result after matching.

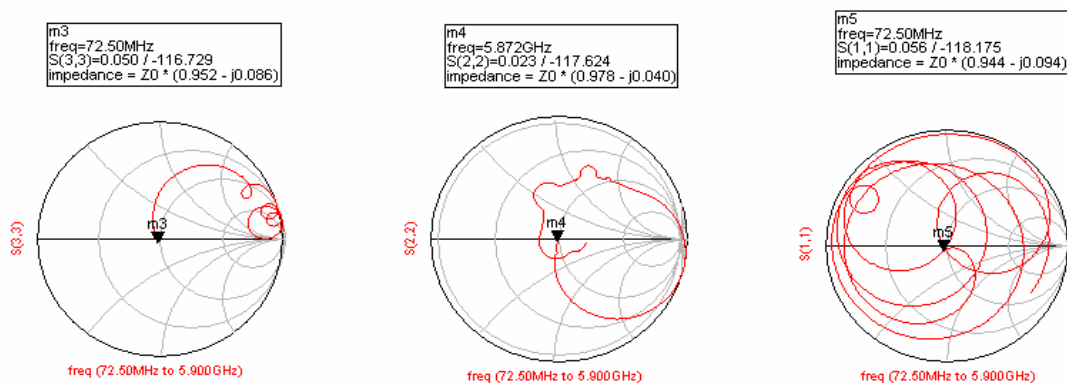


Figure 22: S-parameters simulation after matching

### 7.1.3 Stepped impedance lowpass filter

The order of the filter has been chosen to 5. The requirement of the filter is 20 dB return loss Chebyshev filter and operate in a  $50 \Omega$  system. In addition the electrical lengths of the UEs are chosen to be  $30^\circ$  at the band-edge. Then the  $a$  becomes:

$$a = \sin(w_0) = \sin(30^\circ) = 0.5$$

To calculate the element values the following steps has been made:

$$h = \sinh \left[ \frac{1}{N} \sinh^{-1} \left( \frac{1}{e} \right) \right]$$

Where  $e$  is defined in the worst case as following:

$$\text{Insertion loss} = 10 \log(1 + e^2) = 10 \log \left( \frac{1}{|S_{12}|^2} \right)$$

And

$$\text{Return loss} = 10 \log \left( \frac{1}{|S_{11}|^2} \right) = L_R$$

Then

$$|S_{11}|^2 = 10^{-L_R/10} \text{ and } |S_{12}|^2 = 1 - |S_{11}|^2$$

According to the requirements:

$$N = 5$$

$$L_R = 20 \text{ dB}$$

Then  $e = 0.1005$ , which means that  $h$  will be 0.635.

The formulas for this stepped impedance filter have been developed and the results for a Chebyshev response are given below:

$$\begin{aligned} Z_r &= 1/g_r \text{ (r odd)} \\ Z_r &= g_r \text{ (r even)} \end{aligned}$$

For  $r = 1, \dots, N$

$$g_r = A_r \left( \frac{2 \sin[(2r-1)p/2N]}{a} - \frac{a}{4} \left\{ \frac{h^2 + \sin^2(rp/N)}{\sin[(2r+1)p/2N]} + \frac{h^2 + \sin^2[(r-1)p/N]}{\sin[(2r-3)p/2N]} \right\} \right)$$

Where  $A_r$  are:

$$A_1 = \frac{1}{h} = A_5 = 1.5748$$

$$A_2 = \frac{h}{h^2 + \sin^2(p/5)} = A_4 = 0.8481$$

$$A_3 = \frac{h^2 \sin^2(p/10)}{h[h^2 + \sin^2(p/5)]} = 0.90158$$

According to the formulas in the  $50 \Omega$  system the following impedances are obtained:

$$Z_1 = Z_5 = 24.74 \Omega \quad Z_2 = Z_4 = 117.45 \Omega \quad Z_3 = 15.43 \Omega$$

### Simulation of stepped impedance lowpass filter

The simulation of the stepped impedance lowpass filter with the parameters above has been done in the ADS simulation program. To get a better idea about how the circuit works the S-parameter simulation has been done.

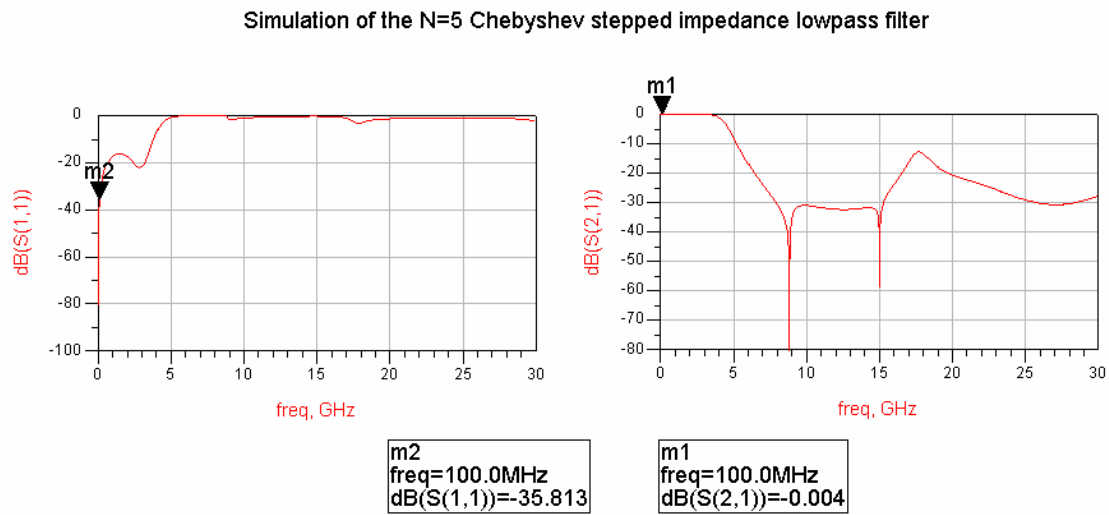


Figure 23: Filter's simulation

## 7.2 Simulation

To yield the best performance an optimization of the circuit has to be done. According to the final result as shown in Figure 24 the gain which can be achieved is 10,485dB since the power at the output port, IF-port is -19.515dB and the input power at the RF-port is approximated to be about -30dB.

Simulation of activemixer at RF=5.8GHz and IF=72.5

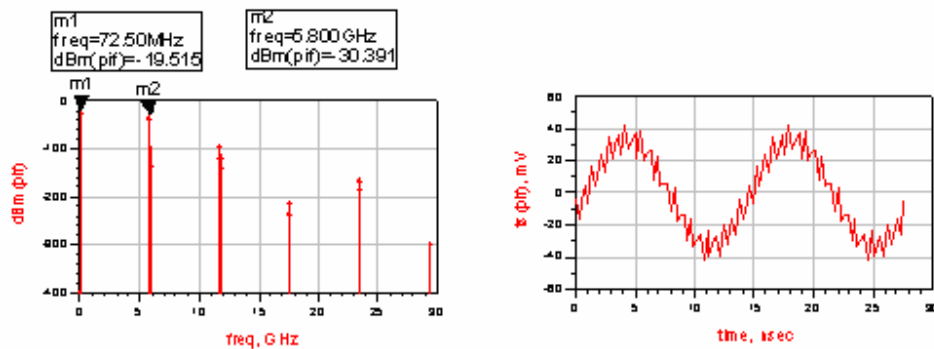


Figure 24: Simulation of the mixer

Figure 25 shows how well matched the input and output ports are at the chosen frequencies. The reflection loss for the RF-port -32.718dB, for the LO-port -29.323dB and for IF-port -25.981dB.

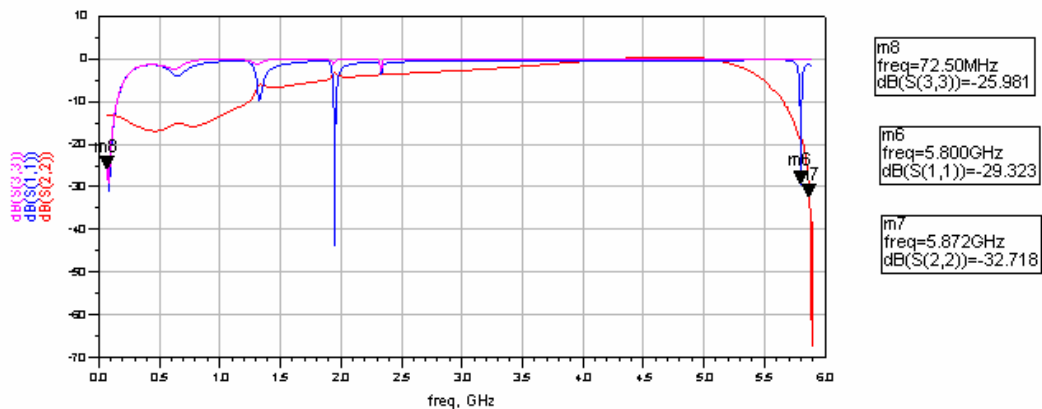


Figure 25: S-parameters as function of frequencies

## 7.3 Construction

Since the impedance value of each section of the filter is known, the physical dimension of the filter can be calculated with ADS line calc. For a better result an optimization has been done. The results are:

**Components for biasing circuit:**

$R_1 = 198 \Omega$   
 $R_2 = 135 \Omega$   
 $R_3 = 100 \Omega$

$V_{cc} = 10 \text{ V}$   
 $V_{bb} = 1.8 \text{ V}$

**Block capacitor and inductor:**

$C_{RF} = 10 \text{ nF}$   
 $L_{CC} = 1 \mu\text{H}$

$C_{LO} = 10 \text{ nF}$   
 $L_{BB} = 1 \text{ nH}$

**Lowpass filter:**

$W_1 = W_5 = 8.00706 \text{ mm}$   
 $W_2 = W_4 = 0.349874 \text{ mm}$   
 $W_3 = 14.502$

$L_1 = L_5 = 2.47524 \text{ mm}$   
 $L_2 = L_4 = 2.83541 \text{ mm}$   
 $L_3 = 2.40631 \text{ mm}$

**Matching circuits:**

RF:

$L_{RF1} = 4.61577 \text{ mm}$   
 $W_{RF1} = 1.14072 \text{ mm}$

$L_{RF2} = 8.90676 \text{ mm}$   
 $W_{RF2} = 0.158844 \text{ mm}$

LO:

$L_{LO1} = 16.6115 \text{ mm}$     $W_{RF1} = 1.14072 \text{ mm}$     $L_{RF} = 1.467 \text{ nH}$

IF:

$C_{IF} = 100 \text{ pH}$     $L_{IF} = 47 \text{ nH}$

The whole mixer layout was made in Protel DXP as show in figure

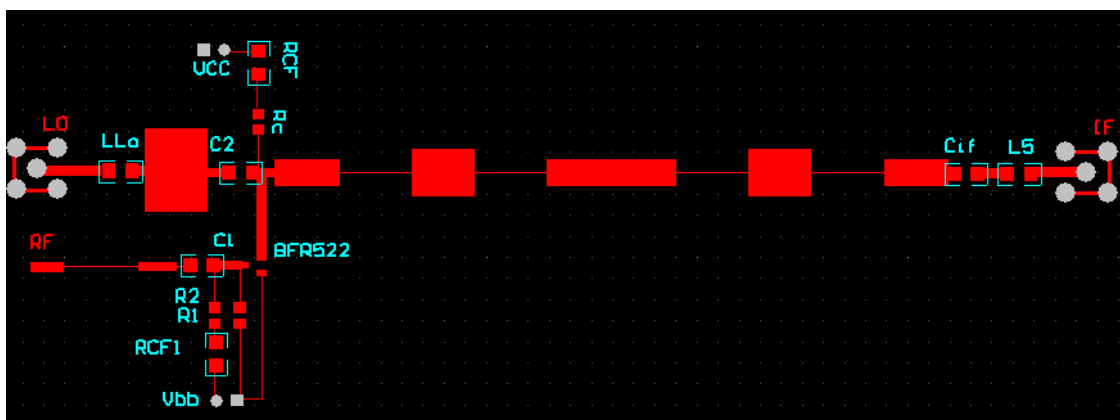


Figure 26: Layout of the mixer

## 8 Active Bandpass Filter

Active filters are circuits that use an operational amplifier (op amp) as the active device in combination with some resistors and capacitors to provide an LRC-like filter performance at low frequencies. One of the active filter model is the multiple feedback active filter shown in Figure 27.

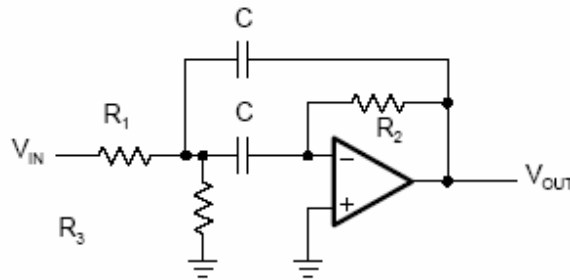


Figure 27: Active filer

### 8.1 Analysis

In order to provide a larger IF-signal an active band pass filter is needed. The specifications of the filter are the following:

Center frequency  $f_m = 72.5$  MHz

Quality factor  $Q = 10$

Gain  $A_m = 20$  dB

The filter design was based on the active feedback filter model with the following transfer function:

$$A(s) = \frac{-\frac{R_2 R_3}{R_1 + R_3} C \omega_m s}{1 + \frac{2R_1 R_3}{R_1 + R_3} C \omega_m s + \frac{R_1 R_2 R_3}{R_1 + R_3} C^2 \omega_m^2 s^2}$$

The capacitor was chosen to a certain value then the resistors can be easily solved. The equations to characterize the multiple feedback active filter are the following:

$$f_m = \frac{1}{2\pi C} \sqrt{\frac{R_1 + R_3}{R_1 R_2 R_3}}$$

$$-A_m = \frac{R_2}{2R_1}$$

$$Q = p f_m R_2 C$$

Theoretical results:

$$C = 1 \text{ pF} \quad R_2 = 43.905 \text{ k}\Omega \quad R_1 = 2.1952 \text{ k}\Omega \quad R_3 = 115.5390 \Omega$$

## 8.2 Simulation

The active multiple feedback band pass filter was simulated in Protel DXP. To start with the simulation was based on the theoretical values, but unfortunately the results were not as expected. To achieve the requirements the capacitor and the resistors had to be changed, giving a simulated absolute gain of about 9dB.

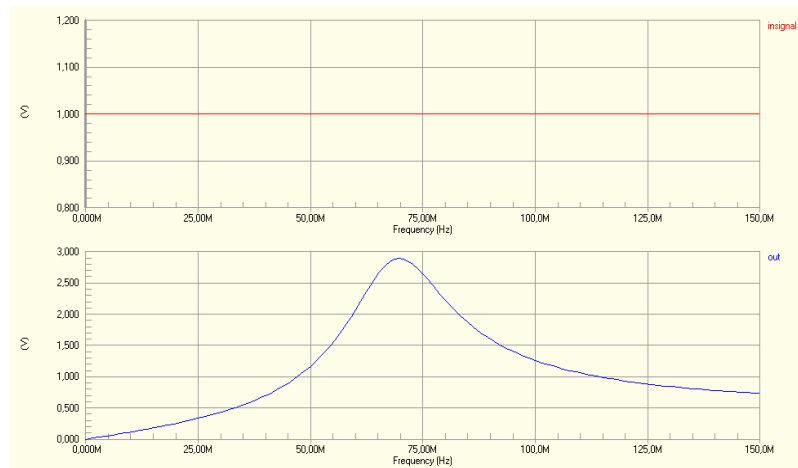


Figure 28: Simulation of the active band pass filter

## 8.3 Construction

The layout for the etching of the filter, see Figure 29, was designed in Protel DXP.

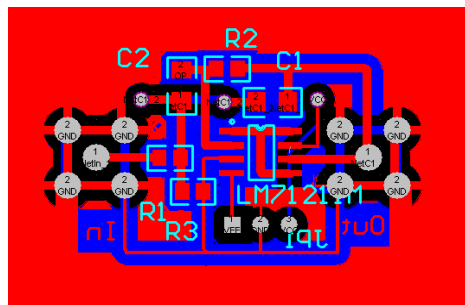
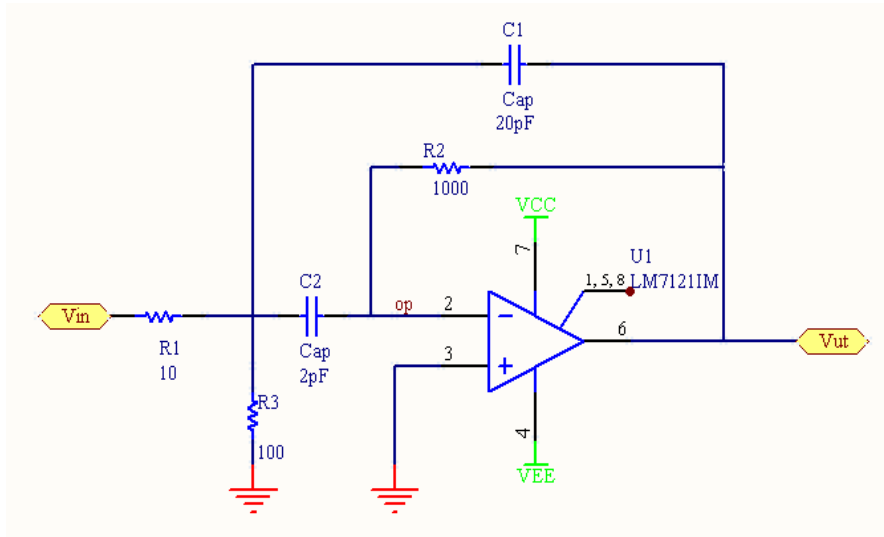


Figure 29: Active band pass filter layout

The values of the components, as seen in Figure 30 are:

$$C_1 = 20 \text{ pF} \quad C_2 = 2 \text{ pF} \quad R_1 = 10 \Omega \quad R_2 = 1 \text{ k}\Omega \quad R_3 = 100 \Omega$$



**Figure 30: Schematic of the active filter at 72.5 MHz**

## 9 Signal Processing

The signal processing part of the system consists of two devices, an ADC (analog to digital converter), and a DSP (digital signal processor) which are connected to the computer via the parallel port. The ADC and DSP that have been used is the AD6600 dual channel IF sampling analog to digital converter and the AD6620 dual channel decimation receiver circuit respectively, produced by Analog Devices. The evaluation boards are inter-connectable, one can test the operation of the DSP combined with the different A/D-converters by just plugging in the desired board, see Figure 31.

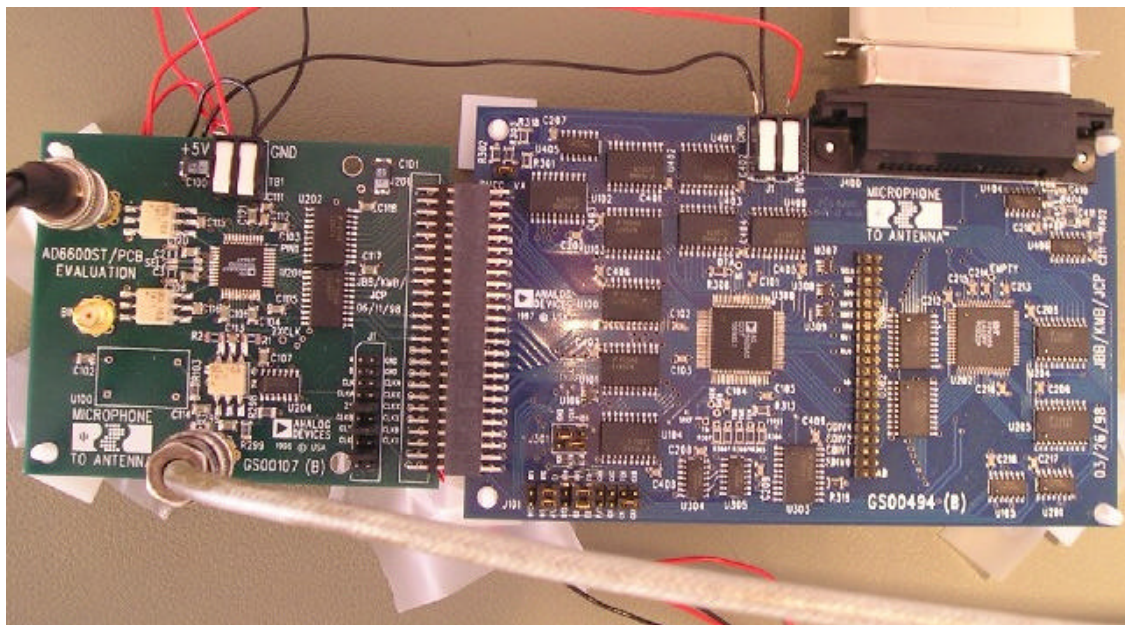


Figure 31: AD6600 and AD6620 evaluation boards

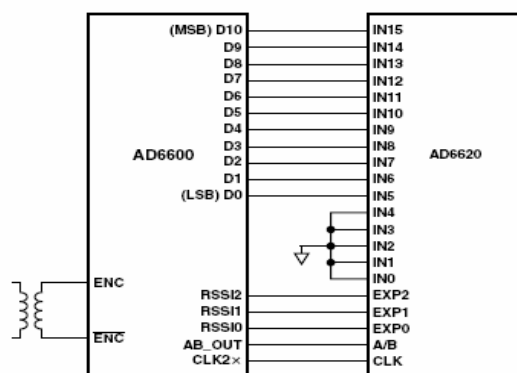


Figure 32: AD6600/AD6620 Connection

## 9.1 Analog to Digital Converter, AD6600

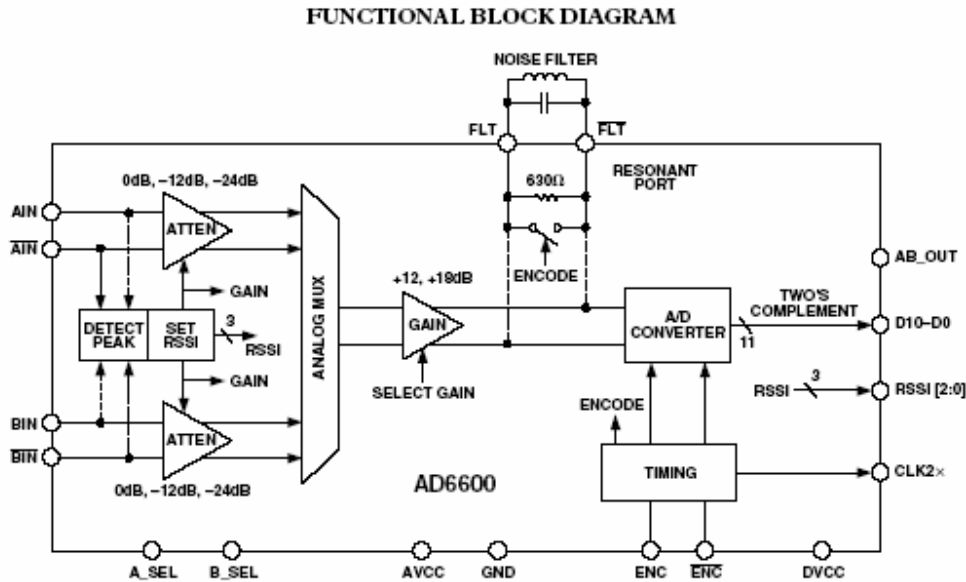


Figure 33

The AD6600 IF signal receiver chip can sample a signal at analog input frequencies up to 250 MHz. The device, Figure 33, contains two input channels, A and B, each with 1 GHz input, 0dB to -24 dB, phase compensated attenuator step, each attenuator is 12 dB. The number of input channels used depends on which application mode is chosen: single mode, dual channel real mode or single channel complex mode. The signal/signals pass through an analog multiplexer which followed by a 12/18 dB gain amplifier. Both channels are sampled with 450MHz track-and-hold followed by an 11-bit, 20 MSPS analog to digital converter. The peak detector monitors the strength of the signal at both input channels.

The peak detector drives the RSSI (received signal strength) circuit that automatically adjusts attenuation and gain on a clock by clock basis and is designed to follow the analog input one clock cycle before the conversion is actually made. Since the peak detector works for a complete cycle prior to conversion, the absolute minimum IF frequency that can be determined is twice the sample rate per channel. Therefore in this system when using the 10 MHz clock the minimum IF frequency that can be sampled would be at least 20 MHz. The more cycles of the input that are monitored by the peak detector, the more accurate the gain setting will be. Therefore the minimum IF should be 70 MHz. In this project the IF,  $f_{CH}$ , is chosen to 72.5 MHz to fulfill the requirements.

## 9.2 Digital Signal Processing, AD6620

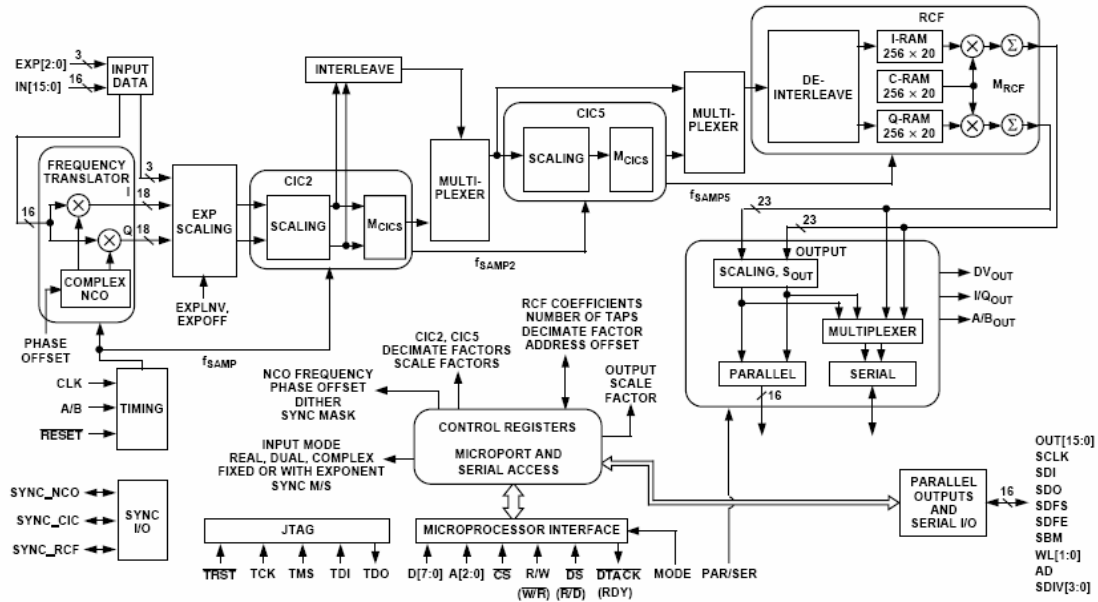


Figure 34: Block Diagram

Figure 34: a frequency translator, two cascaded integrator comb FIR filters (second order cascade integrator comb filter, CIC2, and fifth order cascade integrator comb filter, CIC5) and a RAM Coefficient FIR Filter (RCF). The decimations of the filters,  $M_{CIC2}$  and  $M_{CIC5}$  are calculated by a digital filter design program. The decimation ratio of the RAM Coefficient FIR filter,  $M_{RCF}$  may be programmed from 1 to 32.

The input signal might be real or complex depending on if the chosen mode is single channel real, single channel complex or double channel real. The input data port is sampled on the rising edge of CLK at a maximum rate of 67 MSPS at single channel real or 33.5 at single channel complex and diversity channel real

The frequency translator is implemented with a 32-bit complex numerically controlled oscillator (NCO). The frequency translator translates the incoming digital IF signal to base band.

Decimation filters remove unwanted signals and noise from the incoming signal. Large decimation factors can improve the SNR of ADC by 36 dB or more. Programmable RAM Coefficient filters allows antialiasing

## 9.2.1 Digital filter design

The digital filter has been designed in a filter design program provided by Analog Devices. The filter which has been used has the frequency response in Figure 36. The produced coefficients then can then be programmed into the DSP device.

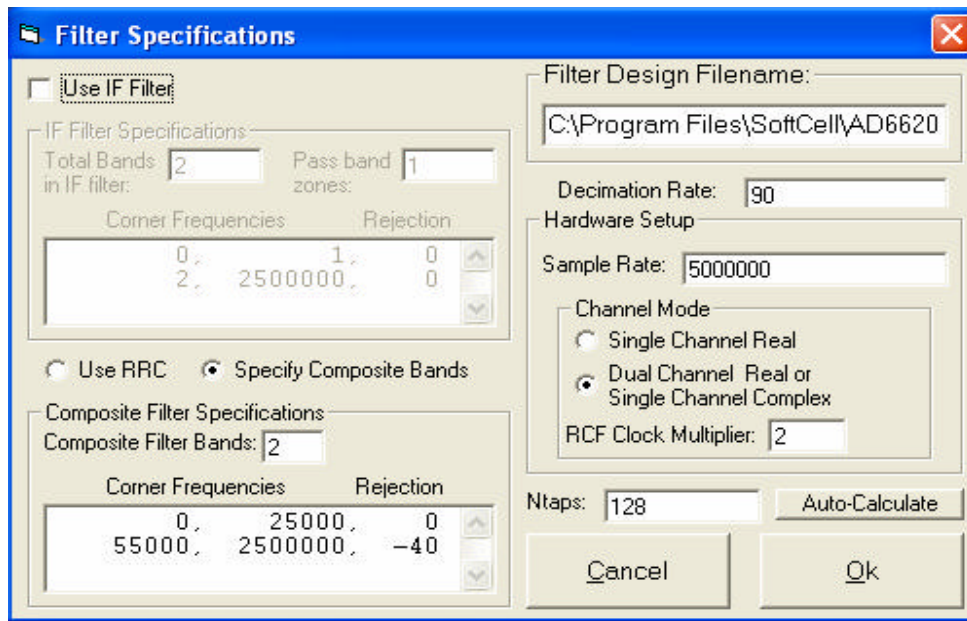


Figure 35: The digital filter requirements

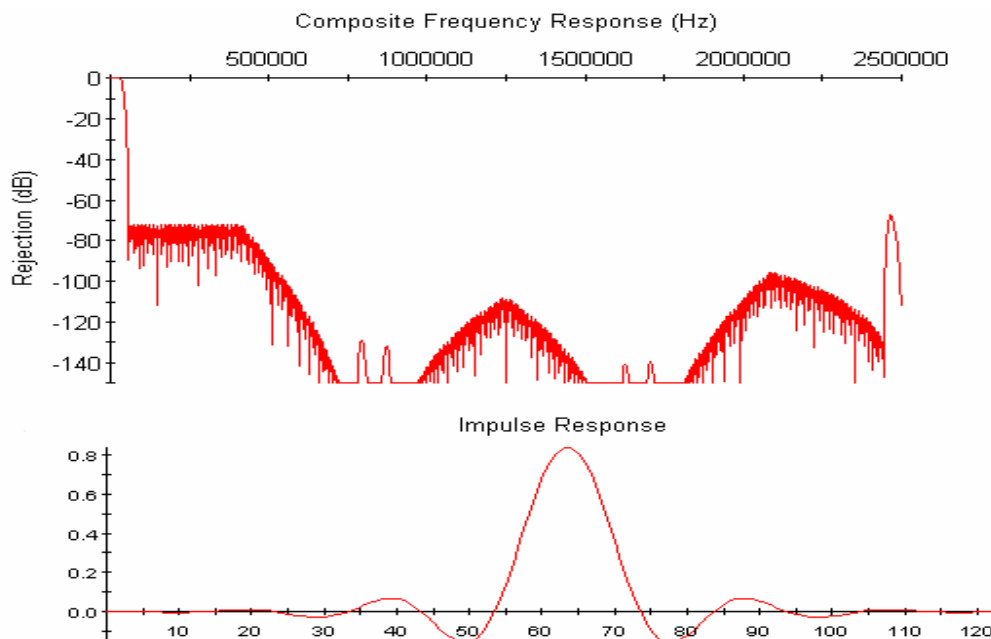


Figure 36: The digital filter response

## 9.3 Software

Since the signal processing software which provided by Analog Devices can only be used online, therefore in order to obtain the data for further signal processing extra software is needed. The software was written by a software engineer.

### 9.3.1 Structure of the interface

In this section the different controls in the main window are described:

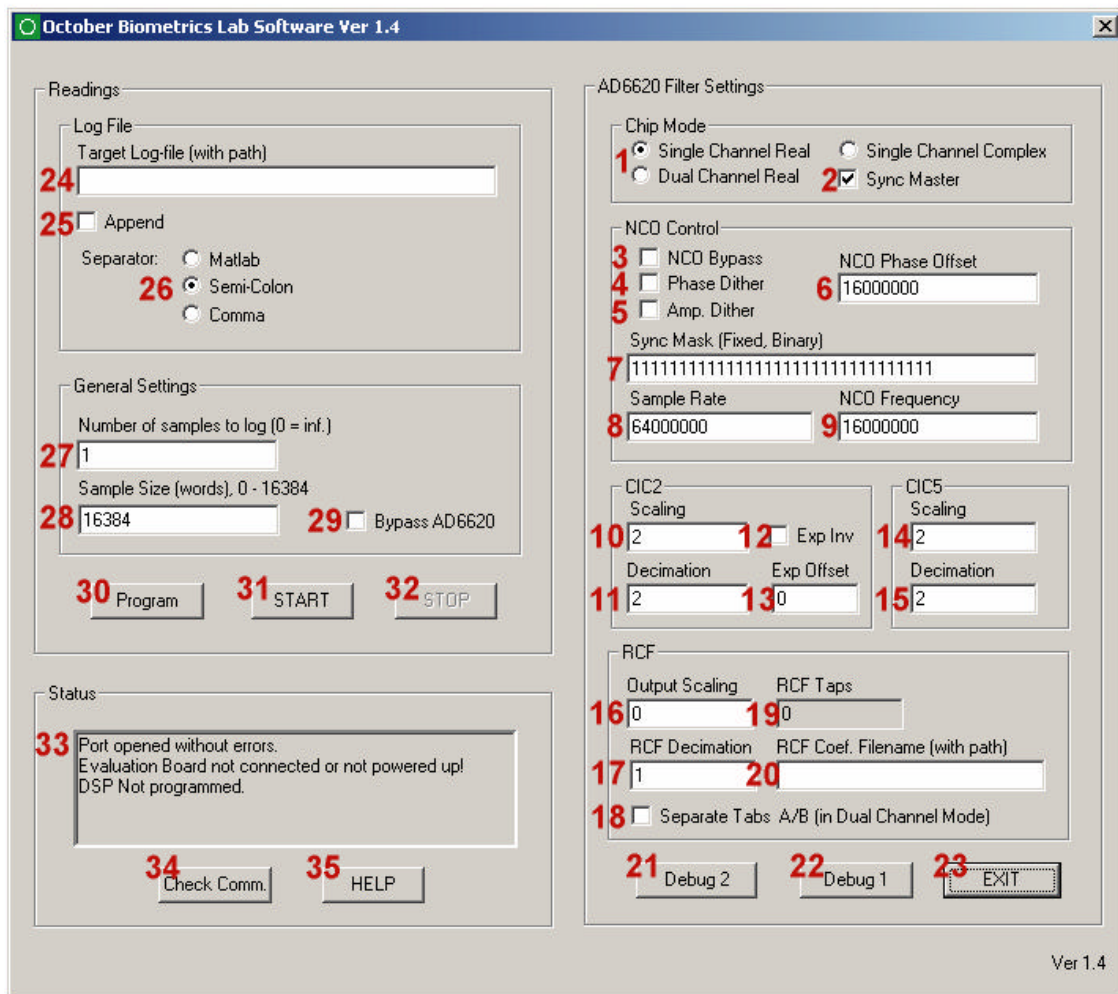


Figure 37: Software interface

**Chip Mode, 1:** Which mode the DSP should operate in. Note that each mode has different demands on input timing etc. (Specifically the A/B input has different meaning in the different modes.) This setting also controls how data is output to the log-file. If the mode is set to dual channel real (sometimes called diversity channel), four rows of data

are output, corresponding to  $I_A$ ,  $Q_A$ ,  $I_B$  and  $Q_B$ . For the single channel modes, output is two rows of data.

**Sync Master, 2:** If this is checked, the DSP is set to be the master in a multi-DSP environment, and it outputs synchronization pulses at certain intervals to let the other DSP:s synch properly. If this control is left unchecked, the DSP will not operate unless it gets the same synchronization signals to the proper inputs.

**NCO Bypass, 3:** If this control is checked, the DSP bypasses the operation of NCO I-Q matching, and the data streamed through the DSP remain pure A/D-data.

**Phase Dither, 4:** If this control is checked, phase dither is turned on. Refer to the AD6620 datasheet!

**Amp Dither, 5:** If this control is checked, amplitude dither is turned on. Refer to the AD6620 datasheet!

**NCO Phase Offset, 6:** Allow the user to enter the AD6620 NCO Phase Offset (0 to 65535).

**Sync Mask, 7:** This setting is relevant when the DSP is operating in a multi-DSP environment, and should normally be left to all ones. Refer to AD6620 datasheet for full specification.

**Sample rate, 8:** User sets the clock rate the AD6620. This should indicate the clock frequency per channel.

**NCO Frequency, 9:** The NCO frequency is half of the sample rate.

**Decimation rate, 11 and 15:** These coefficients are automatically updated when the digital filter is chosen

**Scaling, 10 and 14:** Since the decimations are fixed coefficients depending on the specification of the filter parameters, and to avoid overflow, the scale factors of the filters are chosen according to the equations below:

$$S_{CIC2} = \text{ceil}(\log_2(M_{CIC2}^2 \times \text{input\_level}))$$

$$OL_{CIC2} = \frac{1}{2^{S_{CIC2}}} \times \text{input\_level}$$

$$S_{CIC5} = \text{ceil}(\log_2(M_{CIC5}^5 \times OL_{CIC2})) - 5$$

$$OL_{CIC5} = \frac{1}{2^{S_{CIC5}}} \times OL_{CIC2}$$

**Exp.Inv, 12:** Used with the AD6600 gain ranging ADC. Inverts the exponents (RSSI) bits when checked.

**Exponent Offset, 13:** Used with AD6600 gain ranging ADC. Sets the number of gain ranges the data is offset by. For the AD6600 this should be set to 6.

**Target Log-file (with path), 24:** The place where the log-file will be stored.

**Separator, 25:** The type of the log-file depending on what the user wants.

**Readings Index, 26:** The number of times each antenna is active.

**Antenna Index, 27:** The amounts of the antenna

**Sample Size, 28:** The number of samples in each scan.

## 10 Synchronisation

There are two computers involved in the measurements. The first computer is controlling a stepper motor. The stepper motor is used to transporting the object (ex: baby food) in the measurement gap. The second computer is used for the data acquisition.

It's quite important that both, the movement and the data acquisition start at same time i.e. synchronised. To accomplish that, three digital circuits have been designed see appendix. The selections of antennas were achieved by the mean of 4 microwave switches.

# 11 Power Supply

A power supply providing 3.4 V has been built. This power supply is used to power the DSP unit. Figure 38 shows the circuit schematic and the simulation result for the power supply. Two Zener diodes have been used to step down the voltage in tow stages.

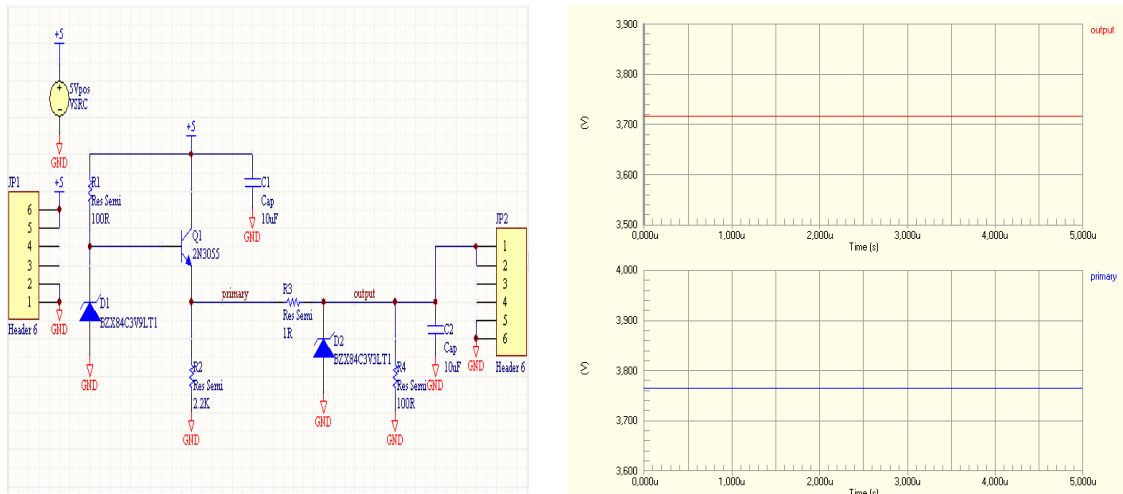


Figure 38: Circuit schematic and simulation result for the power supply

## 12 Results

One of the objectives of this master thesis work was to verify whether the 3D-microwave tomography system which has been built functions as expected or not. To accomplish that a lot of measurements (about two thousands) have been conducted. The measurements included both foreign body detection and temperature measurement.

To examine the ability of the system different materials have been used as test object. For foreign body detection food materials like bread loaf, raisins, spices, and baby food were examined. For temperature measurement application water and play-doh have been used.

The obtained results for the foreign body detection were impressive, since varies foreign bodies such as metal, glass and plastic with different shapes and small dimensions down to 2mm could be detected. Figure 39 shows a plot of raw data from 8 runs. As it can be seen there is a clear difference between the clean and the contaminated product.

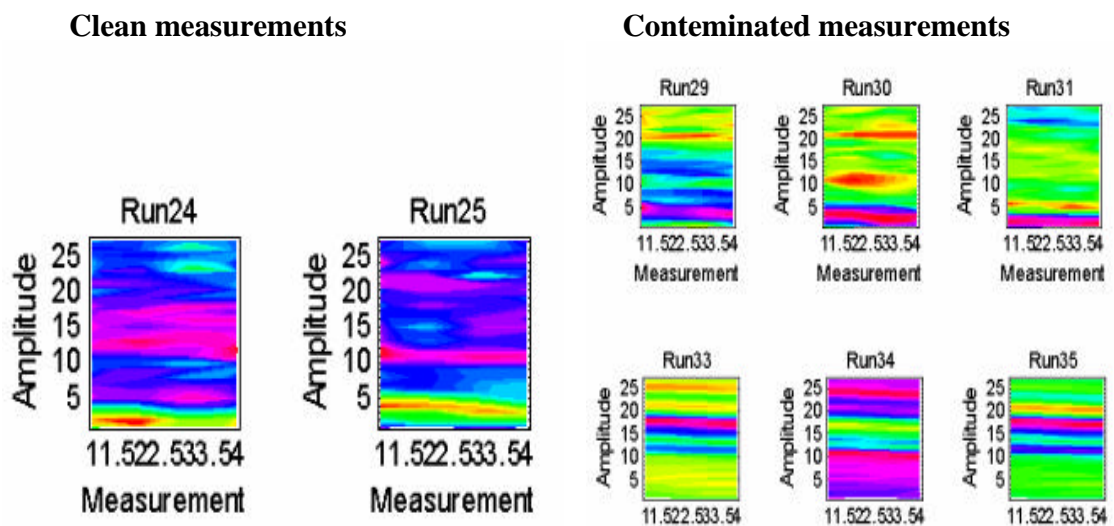


Figure 39: Plot of raw data

To have a better understanding, the results can be presented as shown in Figure 40. To begin with in order to obtain the level of the threshold line, many measurements for a “clean” product should be conducted. The mean value of the measurements and the required security level will decide the position of the line. The position of the threshold line can updated after each clean product detection. If the mean value of each run situated above the threshold line then the product is contaminated.

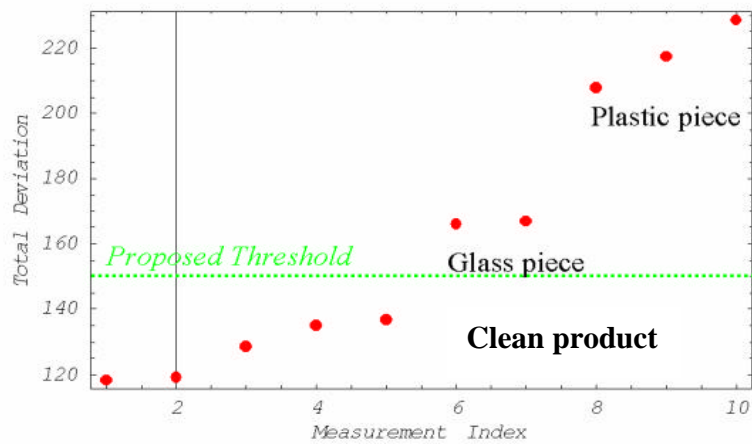


Figure 40: Plot of baby food measurements

## 13 Conclusions

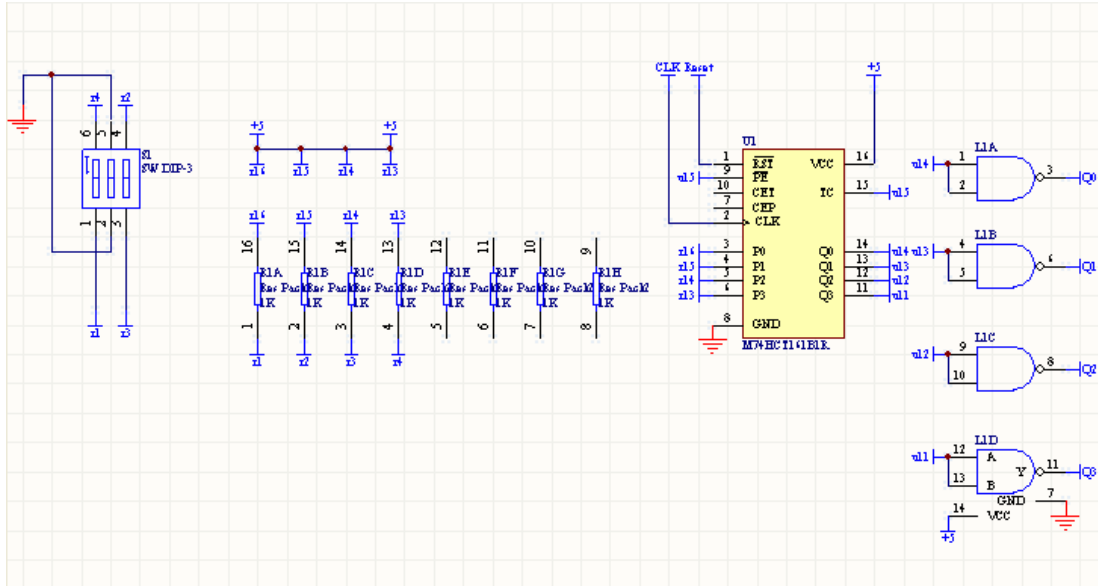
The results were promising in a way that give one the courage to say that it is worth it to go on with the project. However, there is always room for improvement in any system and ours is no different. While we have managed to produce a fully functional, complete system there are plenty of improvements and additions that are possible. The following is a summary of what it is seen to be the most beneficial improvements and additions to the system:

1. Hardware that can replace the computers and improve the data acquisition and signal processing. That makes the scanning process faster and more suitable for industry environment.
2. Replace the microwave generators with PLLs.
3. Integrated the antennas with the rest of the system.
4. EMC housing and assemble the system in a stainless steel box to stand the tough industry environment

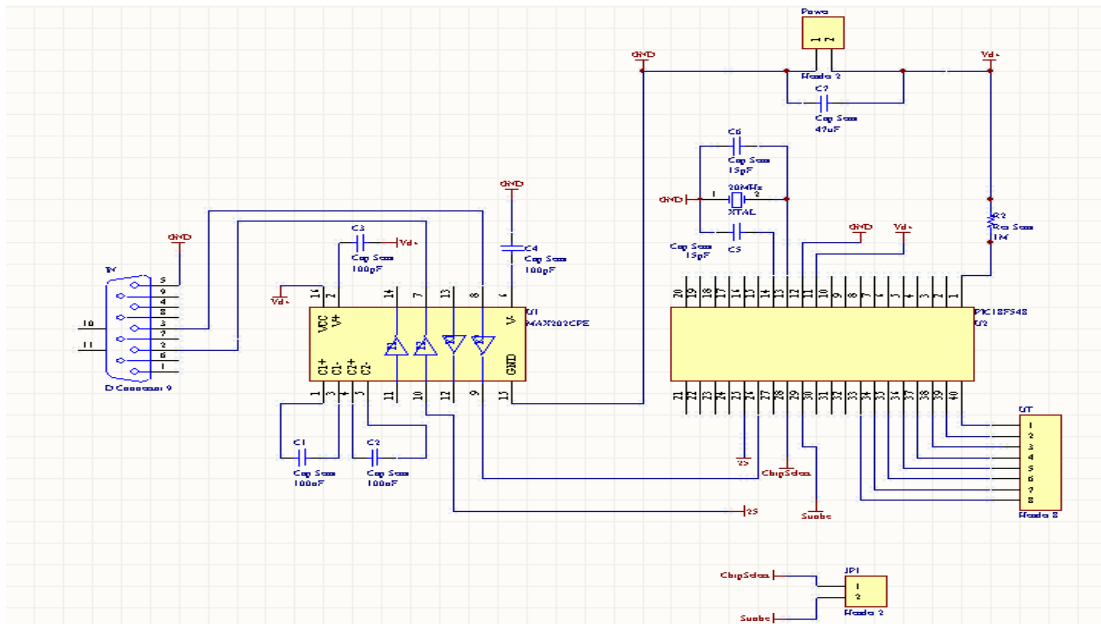
## 14 References

- [1] Constantine A. Balanis, Antenna theory analysis and design, second edition, Wiley, New York, 1997.
- [2] G.T. Herman, S.P. Célestin, Basic methods of tomography and inverse problems a set of lectures, Hilger, Bristol , 1987.
- [3] I. Hunter, Theory and design of microwave filters, Institution of Electrical Engineers, London, 2001.
- [4] R.E. Collin, Foundations for microwave engineering, second edition, McGraw-Hill, New York, 1992.
- [5] <http://cws.gateway.tec.wi.us/faculty/hoppep/Active%20Filter%20Design.pdf>
- [6] <http://www.ee.bilkent.edu.tr/~microwave/programs/magnetic/dcoupler/theory.htm>

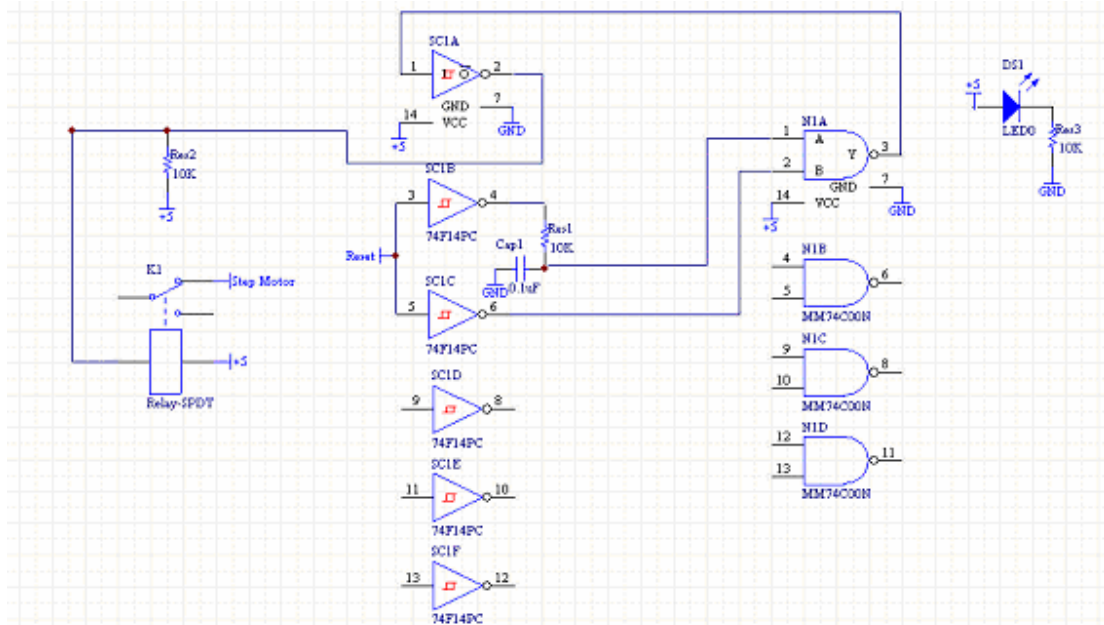
# 15 Appendix



Antenna switching control circuit



Clock and reset signal generator circuit



Stepper motor controller circuit